



# THE 1:2 MODE INTERACTION IN RAYLEIGH–BÉNARD CONVECTION WITH AND WITHOUT BOUSSINESQ SYMMETRY

JOANA PRAT

*Departament de Matemàtica Aplicada IV,  
Universitat Politècnica de Catalunya, Barcelona, Spain*

ISABEL MERCADER

*Departament de Física Aplicada, Universitat Politècnica de Catalunya,  
Barcelona, Spain*

EDGAR KNOBLOCH

*Department of Applied Mathematics, University of Leeds, Leeds LS2 9JT, UK*

Received February 8, 2001; Revised April 6, 2001

Nonlinear two-dimensional Rayleigh–Bénard convection with periodic boundary conditions in the horizontal is studied for spatial periods near the 1:2 steady state mode interaction. The boundary conditions at the bottom are no-slip, and convection is driven by a fixed imposed temperature difference across the layer. Homotopic continuation is used to continue the boundary conditions at the top from no-slip ( $\beta = 0$ ) to stress-free ( $\beta = 1$ ). When  $\beta = 0$  and non-Boussinesq effects are absent the system has midplane reflection symmetry and the 1:2 resonance is weak. When  $\beta = 1$  this symmetry is strongly broken and the resonance is strong. The transition between these two cases is explored for two Prandtl numbers,  $\sigma = 10$  and  $\sigma = 0.1$ , representing behavior typical of large and low Prandtl numbers, respectively.

## 1. Introduction

Midplane reflection symmetry plays a profound role in the theory of Rayleigh–Bénard convection in both two and three dimensions. In three dimensions this symmetry identifies up- and down-hexagons so that the appearance of a particular hexagon type is necessarily a consequence of initial conditions [Golubitsky *et al.*, 1984; Clever & Busse, 1996]. The marked preference for one or other type of hexagons observed in experiments is a consequence of the breaking of the midplane reflection symmetry either by non-Boussinesq effects [Busse, 1967] or by differences in the boundary conditions at the top and bottom of the fluid layer. The effects of midplane reflection on convection in two spatial dimensions are less well known. However, in an earlier paper

Prat *et al.* [1998] pointed out, following Busse and Or [1986] and Armbruster [1987], that the presence of midplane reflection symmetry (hereafter Boussinesq symmetry) changes the structure of mode interactions even in two dimensions, provided only that the resonant terms in the corresponding amplitude equations are even. This effect is particularly dramatic in the 1:2 resonance because with symmetry this resonance is weak, i.e. the resonant terms are of fifth order. In contrast, as discussed by Mercader *et al.* [2001a], when this symmetry is appropriately broken the behavior characteristic of the strong 1:2 resonance [Armbruster *et al.*, 1988; Jones & Proctor, 1987; Proctor & Jones, 1988] is restored. This occurs already for quite small values of the symmetry-breaking parameter  $\beta$ . In the present

paper we extend the work of Mercader *et al.* and homotopically continue the velocity boundary conditions at the top of the layer from no-slip ( $\beta = 0$ ) to stress-free ( $\beta = 1$ ) in order to elucidate the origin of the various solution branches present in the latter case, and their relation to the solution branches in the symmetric case  $\beta = 0$ . Two values of the Prandtl number are used,  $\sigma = 10$  and  $\sigma = 0.1$ , characteristic of high and low Prandtl number fluids. In both cases the sequence of transformations that connects the symmetric and nonsymmetric cases is exceedingly rich. It should be noted that the effects on the 1:2 resonance of small non-Boussinesq terms (equivalent to small nonzero values of our parameter  $\beta$ ) were studied by Manogg and Metzener [1994] from a similar point of view, while Cox [1996] considered the long wave equations governing convection between nearly insulating boundaries with different combinations of stress-free and no-slip boundaries at the top and bottom. However, neither of these papers studied the sequence of transitions that must take place as the symmetry is increasingly broken. Some idea of the complexity of these transitions can be gleaned from the work of Porter and Knobloch [2001] on the 1:2 resonance with  $O(2)$  symmetry; this work examines, in the context of the corresponding amplitude equations, the effect of changing the relative magnitude between the resonant quadratic terms and the non-resonant cubic terms.

In the present paper we choose one particular way of breaking the Boussinesq symmetry, applying homotopic continuation to the velocity boundary conditions. This procedure has the advantage over other ways (e.g. including non-Boussinesq terms, or introducing a Biot number into the temperature boundary conditions) in that the basic (conduction) state remains unchanged. We expect, however, that the sequence of transitions described below is typical of other ways of breaking the Boussinesq symmetry as well, although some of the details may well differ.

The paper is organized as follows. In Sec. 2 we summarize the equations and boundary conditions employed. The results obtained by numerical continuation for different values of the symmetry-breaking parameter  $\beta$  are presented in Sec. 3. Some of the higher codimension bifurcations uncovered in Sec. 3 are analyzed in Sec. 4, and related to the numerical results of Sec. 3. The paper concludes with a brief discussion.

## 2. Basic Equations

We consider two-dimensional Boussinesq thermal convection in a periodic horizontal layer, and compute both steady convecting states and steady traveling wave states in the nonlinear regime. Since both tilted convection rolls and the traveling waves are associated with a nontrivial mean flow, we split the solenoidal velocity field  $\mathbf{v}(x, z, t)$  into its mean and fluctuating components,

$$\mathbf{v} = \mathbf{U}(z, t) + \mathbf{v}'(x, z, t),$$

where  $\mathbf{U} = (U, 0)$ ,  $\mathbf{v}' = (-\partial_z \chi', \partial_x \chi')$  and  $\overline{\mathbf{v}'} = \overline{\chi'} = 0$ , with the overline indicating an average over the horizontal period. The temperature  $T(x, z, t)$  is written in the nondimensional form

$$T = \frac{1}{2} - z + \theta(x, z, t).$$

Equations for  $U$ ,  $\chi'$  and  $\theta$  are obtained from the horizontal average of the Navier–Stokes equations, the deviation of the vorticity equation from its horizontal average and the heat equation. In nondimensional form these are

$$(\partial_t - \sigma \partial_{zz}^2)U + \partial_z \overline{v'_x v'_z} = 0, \quad (1a)$$

$$\begin{aligned} (\partial_t + U \partial_x - \sigma \nabla^2) \omega' + Ra \sigma \partial_x \theta + \partial_{zz}^2 U \partial_x \chi' \\ + \frac{\partial(\chi', \omega')}{\partial(x, z)} - \overline{\frac{\partial(\chi', \omega')}{\partial(x, z)}} = 0, \end{aligned} \quad (1b)$$

$$(\partial_t + U \partial_x - \nabla^2) \theta - \partial_x \chi' + \frac{\partial(\chi', \theta)}{\partial(x, z)} = 0, \quad (1c)$$

where  $\omega' = -\nabla^2 \chi'$ , lengths and time have been expressed in units of the layer depth and thermal diffusion time in the vertical, respectively, and  $Ra$  and  $\sigma$  are the Rayleigh and Prandtl numbers. The boundary conditions are taken to be periodic in  $x$  with period  $L$ . The top and bottom boundaries are perfectly conducting,

$$\theta = 0 \quad \text{at} \quad z = \pm \frac{1}{2}, \quad (1d)$$

with the velocity boundary conditions

$$\begin{aligned} \beta \partial_z U + (1 - \beta)U &= \chi' \\ &= \beta \partial_{zz}^2 \chi' + (1 - \beta) \partial_z \chi' \\ &= 0 \quad \text{at} \quad z = \frac{1}{2}, \end{aligned} \quad (1e)$$

and

$$U = \chi' = \partial_z \chi' = 0 \quad \text{at } z = -\frac{1}{2}. \quad (1f)$$

The equations are thus defined on the domain  $(x, z) \in [0, L] \times [-1/2, 1/2]$ . The resulting problem is solved numerically for various values of  $\beta$  using a spectral Galerkin–Fourier technique in  $x$  and collocation–Chebyshev in  $z$ . In the following we define the quantity  $\alpha \equiv 2\pi/L$  and compute bifurcation diagrams as a function of  $Ra$  for values of  $\alpha$  on either side of  $\alpha_c$ , the location of the 1:2 resonance. This quantity is determined by the intersection of the  $n = 1$  and  $n = 2$  neutral stability curves for the conduction state (cf. [Mercader *et al.*, 2001a]) and depends on  $\beta$  as shown in Fig. 1, although it is independent of the Prandtl number. For  $\beta = 0$  (corresponding to the presence of Boussinesq symmetry) the mode interaction point is located at  $(Ra_c, \alpha_c) \approx (2022, 2.165)$ .

Insight into the results can be gained by considering the symmetries of the basic states that emerge from the conduction state as  $Ra$  is increased, and the (usually smaller) symmetries of states created in subsequent (secondary) bifurcations. These symmetries depend on the presence or absence of the midplane reflection symmetry. When  $\beta = 0$  Eqs. (1) are equivariant under the two reflections,

$$R_0 : (x, z) \rightarrow (-x, z), \quad (U, \chi', \theta) \rightarrow (-U, -\chi', \theta), \quad (2a)$$

$$\kappa : (x, z) \rightarrow (x, -z), \quad (U, \chi', \theta) \rightarrow (U, -\chi', -\theta), \quad (2b)$$

as well as translations through a distance  $\ell$ ,

$$T_\ell : (x, z) \rightarrow (x + \ell, z), \quad (U, \chi', \theta) \rightarrow (U, \chi', \theta). \quad (2c)$$

The reflection (2a) is with respect to an arbitrarily chosen origin in  $x$ ; reflections  $R_{\ell_0}$  with respect to a plane  $x = \ell_0$ , say, are obtained by conjugation:  $R_{\ell_0} = T_{\ell_0} R_0 T_{-\ell_0}$ . These symmetries generate the symmetry group  $\Gamma = O(2) \times Z_2$ . The conduction state  $U = \chi' = \theta = 0$  is invariant under this group. The primary instability of this state is to a nontrivial roll state  $(0, \chi', \theta)$  that breaks the translation symmetry  $T_\ell$  but is invariant under a reflection  $R_{\ell_0}$  for an appropriate  $\ell_0$  and the *shift-reflect* operation  $T_{a/2}\kappa$ , where  $a \equiv L/n$  is the pattern wavelength [Prat *et al.*, 1998]. Each of these symmetries is a generalized reflection in the sense that its square is the identity. It follows that the symmetry group of such a roll state is  $G \equiv Z_2 \times Z_2 = D_2$ , a subgroup of  $O(2) \times Z_2$  [Weiss, 1990; Moore *et al.*, 1991; Prat

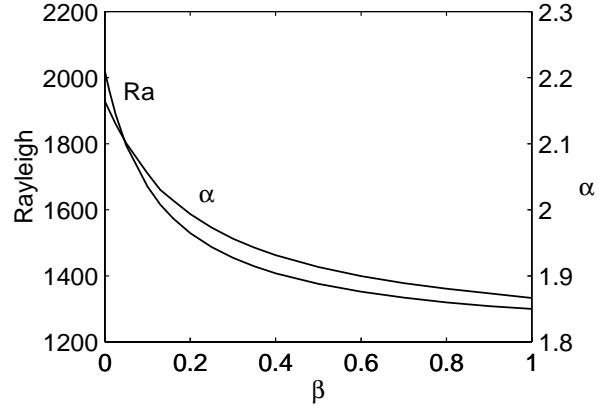


Fig. 1. The dependence of the critical values  $Ra_c$  and  $\alpha_c$  for the 1:2 resonance on the homotopy parameter  $\beta$ . Here  $\alpha = 2\pi/L$  and  $L$  is the imposed spatial period, when  $\beta = 0$ ,  $Ra_c = 2021.6$ ,  $\alpha_c = 2.1648$ .

*et al.*, 1995]. In contrast an individual roll is invariant only under a  $180^\circ$  rotation. For a pattern with a node at  $x = 0$  this symmetry is  $P = R_{a/4}\kappa$  and is sometimes referred to as a *point* symmetry. This symmetry acts on the fields as follows:

$$P : (x, z) \rightarrow \left(\frac{a}{2} - x, -z\right), \quad (2d)$$

$$(U, \chi', \theta) \rightarrow (-U, \chi', -\theta).$$

Note that  $P = R_0 T_{a/2} \kappa$  (since  $T_{\ell_0} R_0 T_{-\ell_0} = R_0$ ) and so  $P \in G$ . In the following we shall use the symbol  $R$  to refer to the reflection  $R_{\ell_0}$  for *suitable*  $\ell_0$ .

When  $\beta > 0$  the reflection  $\kappa$  is broken and  $\Gamma = O(2)$ . The symmetry of the primary flow is thus  $G \equiv Z_2$ , i.e.  $R$  [Crawford & Knobloch, 1991]. In either case the symmetry  $R$  of the primary flow implies that no mean flow is present:  $U(z) \equiv 0$ . This is not necessarily so for the states produced in secondary bifurcations from the primary rolls, if these break the symmetry  $R$  of the roll state.

When  $\beta = 0$  the presence of the  $D_2$  symmetry implies that a roll state of wavelength  $a$  can be written in the form

$$\chi'(x, z) = \sum_{k=1}^K \sum_{m=0}^M \chi_{km} f_m(2z) \sin \frac{2\pi kx}{a}, \quad (3a)$$

$$\theta(x, z) = \sum_{k=0}^K \sum_{m=0}^M T_{km} g_m(2z) \cos \frac{2\pi kx}{a}, \quad (3b)$$

relative to a suitable origin. Here  $k + m$  is odd, and the functions  $f_m(2z)$ ,  $g_m(2z)$  are suitable combinations of Chebyshev polynomials satisfying the boundary conditions. These functions are odd when

$m$  is odd and even when  $m$  is even. The linear stability of such a roll state is determined as in [Prat *et al.*, 1995, 1998]. When  $\beta = 0$  the possible perturbations split into four disjoint classes, those that are invariant under the full group  $G \equiv D_2$ , and those that are invariant under the three nontrivial subgroups of  $G$  generated by the generalized reflections  $P$ ,  $T_{a/2\kappa}$  and  $R$ , respectively [Prat *et al.*, 1998]. A zero eigenvalue with respect to perturbations of the first type indicates a saddle-node bifurcation. The next two classes of perturbations, invariant under  $P$  and  $T_{a/2\kappa}$ , generate solutions with anti-symmetric and symmetric mean flow profiles  $U(z)$ , respectively. Steady state bifurcations of this type produce secondary branches of tilted cells, and of traveling waves. The remaining perturbation type results in a bifurcation to a secondary branch of solutions that are invariant under  $R$ ; such solutions are not associated with a mean flow. Note that these conclusions apply to *fully* nonlinear roll states. Furthermore, expansions of the form (3) can be used to compute the primary branches of solutions with wavelength  $a$  even in the case  $\beta \neq 0$ ; in this case  $k + m$  is either odd or even, depending on the field, while  $f_m$  is neither.

The considerations just described for  $n = 1$ ,  $\beta = 0$ , also apply to the state  $n = 2$ ,  $\beta = 0$ , provided perturbations of period  $L/2$  are considered. This time the symmetry of the basic state is  $D_4$ . Moreover, in a domain of period  $L$  this state can lose stability with respect to perturbations of wavelength  $L$  corresponding to an instability of the  $n = 2$  state with respect to the state  $n = 1$ . Such an instability is a spatial subharmonic instability and is characterized by a Floquet multiplier  $1/2$ , cf. [Prat *et al.*, 1998]. Mathematically, the important point is that it breaks the  $D_4$  symmetry of the  $n = 2$ , and hence corresponds to a steady state bifurcation with double algebraic multiplicity. As a result *two* branches of solutions bifurcate from the  $n = 2$  branch simultaneously. These are the  $R$  and  $P$  states, and both can be found by means of the following expansion:

$$U(z) = \sum_{m=0}^M U_m \tilde{g}_m(2z), \tag{4a}$$

$$\chi'(x, z) = \sum_{k=-K}^K \sum_{m=0}^M \chi_{km} f_m(2z) e^{ik\alpha x}, \tag{4b}$$

$$\theta(x, z) = \sum_{k=-K}^K \sum_{m=0}^M T_{km} g_m(2z) e^{ik\alpha x}, \tag{4c}$$

with  $\chi_{km}$  and  $T_{km}$  now complex and satisfying  $\chi_{-km} = \chi_{km}^*$ ,  $T_{-km} = T_{km}^*$ , and  $\tilde{g}_m = g_m$ . The prime indicates that the  $k = 0$  term is absent. For the  $R$  states  $U_m = 0$ , all  $m$ , while for the  $P$  states  $U_m = 0$  only for  $m$  even. As before, the above expansion (with  $\tilde{g}_m \neq g_m$  and an appropriate change in the functions  $f_m$ ) applies to the case  $\beta \neq 0$  as well. In this case we must distinguish between the two types of  $R$ -symmetric states that now bifurcate *in succession* from the  $n = 2$  state. These are distinguished by an appropriately defined phase difference  $\psi$  between the  $n = 2$  state and the  $n = 1$  perturbation (see [Mercader *et al.*, 2001a]). If  $\psi = 0$  we call the resulting bifurcation point  $M_0$ ; if  $\psi = \pi$  we call it  $M_\pi$ . The former bifurcation point gives rise to solutions that are reflection-symmetric about a nodal line through  $x = 0$ ; the latter have reflection symmetry about the line  $x = L/4$ . In Sec. 4.1 we describe another characterization of the points  $M_0$ ,  $M_\pi$ . The stability of the resulting solutions is calculated as for the  $D_2$ -symmetric rolls although the perturbations no longer split into four subgroups.

We restrict the analysis that follows to solutions that are either steady, or that are steady in a suitably moving reference frame, i.e. to traveling waves (hereafter TW). The speed of the frame (the phase velocity  $c$  of the wave) is determined as part of the solution. All of these solutions (including the  $n = 1$  steady state for  $\beta \neq 0$ ) can be computed using the general expansion (4), with  $x$  replaced with  $x - ct$  for the TW; in the latter case none of the expansion coefficients vanish in general. In all cases the symmetry properties guarantee the existence of TW solutions with phase velocity  $\pm c$ ; the sign of  $c$  is therefore arbitrary. The computations employ a Newton–Raphson iterative scheme with  $K \leq 16$ ,  $M \leq 16$  or  $M \leq 24$ . This resolution suffices for the relatively modest values of the Rayleigh number considered because the Prandtl number used is not very small. We do not follow branches of standing waves and of two-frequency states, although in several cases the corresponding Hopf bifurcations have in fact been detected (see below).

There is a fundamental reason for computing TW in problems of this type. This is because the breaking of the midplane reflection  $\kappa$  allows some of the secondary steady solutions to drift [Matthews *et al.*, 1992; Knobloch, 1996]. This is the case for the point-symmetric solutions  $P$  but not for the solutions with the symmetries  $R$  or  $G$  since both of these retain the symmetry  $R$  even with broken midplane reflection symmetry (see Sec. 4). However,

TW can be produced in a secondary bifurcation even when  $\beta = 0$ , provided the instability breaks both the  $R$  and  $P$  symmetries that are then present. Of course, when  $\beta > 0$  the shift-reflect symmetry of this state is lost but it remains a traveling wave. More details about the symmetries of the possible secondary solution branches can be found in [Prat *et al.*, 1998].

### 3. The Bifurcation Diagrams

This section is divided in four subsections, for  $\alpha > \alpha_c$  and  $\alpha < \alpha_c$  in each of the cases  $\sigma = 10$  and

$\sigma = 0.1$ . In each case we first summarize the results in schematic form, since the quantitative results often mask some of the important details. Since the mode interaction point depends on the values of the symmetry-breaking parameter  $\beta$  we vary in each case the values of  $\alpha$  along with  $\beta$  in order to remain in the vicinity of the mode interaction point  $\alpha_c(\beta)$ .

#### 3.1. The case $\sigma = 10$ : $\alpha > \alpha_c$

Figure 2 shows the sequence of bifurcation diagrams encountered as  $\beta$  increases from  $\beta = 0$  to  $\beta = 1$ , focusing on the diagrams of particular interest. In

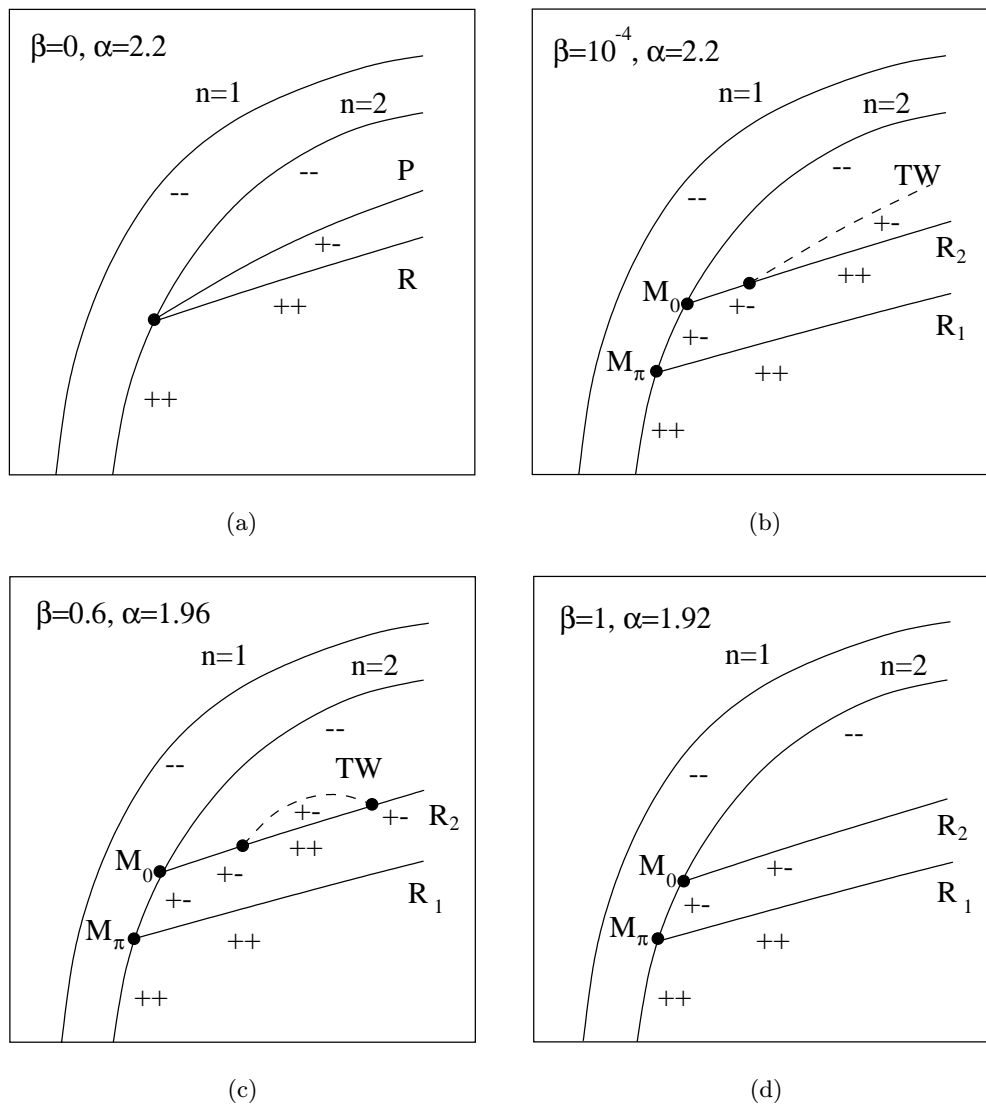


Fig. 2. Schematic bifurcation diagrams for  $\sigma = 10$  and  $\alpha > \alpha_c$ . (a)  $\alpha = 2.2$ ,  $\beta = 0$ , (b)  $\alpha = 2.2$ ,  $\beta = 10^{-4}$ , (c)  $\alpha = 1.96$ ,  $\beta = 0.6$ , (d)  $\alpha = 1.92$ ,  $\beta = 1$ . The solid (dashed) lines denote steady (traveling) solutions. Secondary bifurcations are indicated by solid circles and stability by the signs of the two leading eigenvalues, with + (–) indicating instability (stability). Note that TW are absent both for  $\beta = 0$  and for  $\beta = 1$ .

these diagrams steady solutions are indicated by solid lines, while traveling waves are indicated by dashed lines. The diagrams also indicate the signs of the two dominant eigenvalues, with a minus sign indicating stability. We use the notation  $R_1$  ( $R_2$ ) to refer to the the  $R$ -symmetric branch that bifurcates first (second) from the  $n = 2$  branch as  $Ra$  increases.

For  $\alpha > \alpha_c$  the mode  $n = 1$  sets in prior to  $n = 2$ ; when  $\beta = 0$  the former is a pure mode, but this is no longer the case when  $\beta > 0$ , i.e. when  $\beta > 0$  the  $n = 1$  solutions contain some  $n = 2$  contribution as soon as  $Ra > Ra_c$ . In contrast the  $n = 2$  mode is always a pure mode. For all values of  $\beta$  the  $n = 1$  state bifurcates supercritically with increasing Rayleigh number and remains stable thereafter. However, for larger  $Ra$  these states coexist with stable  $n = 2$  states. When  $\beta = 0$  these states acquire stability at a secondary bifurcation with  $D_4$  symmetry, generated by the two operations  $R$  and  $T_{L/4\kappa}$ ; this group is the symmetry group of a square, with the operation  $R$  identified with a reflection in a line connecting the midpoints of two opposite sides and  $T_{L/4\kappa}$  identified with a  $90^\circ$  rotation. Since this bifurcation involves the  $n = 1$  mode (the bifurcation is *subharmonic*) the  $D_4$  symmetry is broken. As a result the algebraic multiplicity of the zero eigenvalue is two [Crawford & Knobloch, 1991; Bergeon *et al.*, 2001] and the bifurcation produces simultaneously two distinct solution branches. These correspond respectively to the  $P$ - and  $R$ -symmetric states; in the present case both branches are unstable. As soon as  $\beta$  becomes nonzero the  $D_4$  symmetry of the  $n = 2$  states is broken to  $D_2$  (the operation  $T_{L/4\kappa}$  is no longer a symmetry, although  $(T_{L/4\kappa})^2$  is), and hence the multiple bifurcation is split into two successive simple bifurcations to distinct states with the symmetry  $R$ ; the counterpart of the  $P$  states now bifurcates from the  $R_2$  branch in a (tertiary) parity-breaking bifurcation, and takes the form of a drifting state (hereafter a traveling wave, TW). This is the only aspect of the problem where the fact that the  $n = 2$  state is part of a whole circle of states enters into the analysis; as explained by Mercader *et al.* [2001a] the  $P$  states are perturbed into a TW because the symmetry  $\kappa$  that prevented them from drifting along the group orbit is now broken.

Figure 3 shows the quantitative results, including the phase velocity along the TW branch. Observe that for larger  $\beta$  the TW branch no longer extends to large amplitudes but terminates instead

back on the  $R_2$  branch (as shown in Fig. 3(d) for  $\beta = 0.6$ ). With increasing  $\beta$  the resulting TW “bubble” shrinks to zero, and by the time  $\beta$  reaches  $\beta = 1$  [Figs. 3(e) and 3(f)] the TW branch is absent altogether. Thus the  $R$ - and  $P$ -symmetric branches that bifurcate simultaneously from the  $n = 2$  branch when  $\beta = 0$  are replaced by two successive bifurcations to distinct  $R$ -symmetric states when  $\beta = 1$ , with no trace of the  $P$ -symmetric state remaining. Note that the phase velocity of the TW vanishes at the tertiary bifurcations and increases away from them as the square root of the distance from the bifurcation (see, e.g. [Knobloch & Moore, 1990]), and that there is no branch of traveling waves at large amplitude.

### 3.2. The case $\sigma = 10$ : $\alpha < \alpha_c$

Figure 4 shows schematically the corresponding results for  $\alpha < \alpha_c$ . When  $\beta = 0$  and  $\alpha = 2.12$  the  $n = 2$  mode bifurcates first and again remains stable for all values of  $Ra$ . However, there are now two successive bifurcations from the initially unstable  $n = 1$  branch (to  $R$  and  $P$  branches) whose combined effect is to stabilize the  $n = 1$  branch at larger amplitudes. Moreover, a tertiary branch of traveling waves connecting the resulting  $R$  and  $P$  branches is also present, with the TW branch bifurcating from the  $P$  branch at  $Ra = 2145.7$  and connecting to the  $R$  branch at  $Ra = 2145.9$ . We remark that for slightly smaller values of  $\alpha$  the bifurcations to the  $R$  and  $P$  branches trade places and that in this process the TW branch disappears. An example for  $\alpha = 2.08$  can be found in [Prat *et al.*, 1998], Fig. 8(a). Thus the TW are found only very close to the mode interaction point.

For slightly nonzero  $\beta$ ,  $\beta = 10^{-5}$ , the results are noticeably different, largely because of the behavior of the  $n = 1$  branch. This branch becomes a *mixed* mode when  $\beta \neq 0$ , and, as a result, can turn into other mixed mode branches with the same symmetry *without* a bifurcation. As in Fig. 2 the branch  $R$  splits into two steady mixed mode branches  $R_1$ ,  $R_2$  while the  $P$  branch turns into a TW. The lower of the two  $n = 1$  branches consists of an amalgam of the original  $n = 1$  branch and  $R_1$ , and increases monotonically in amplitude. It possesses two secondary bifurcations connected by a secondary TW branch. The resulting bifurcation “bubble” is a consequence of the bifurcation to TW present on the  $R$  branch when  $\beta = 0$ , and consists in part of one of the resulting TW and in part the drifting  $P$  states.

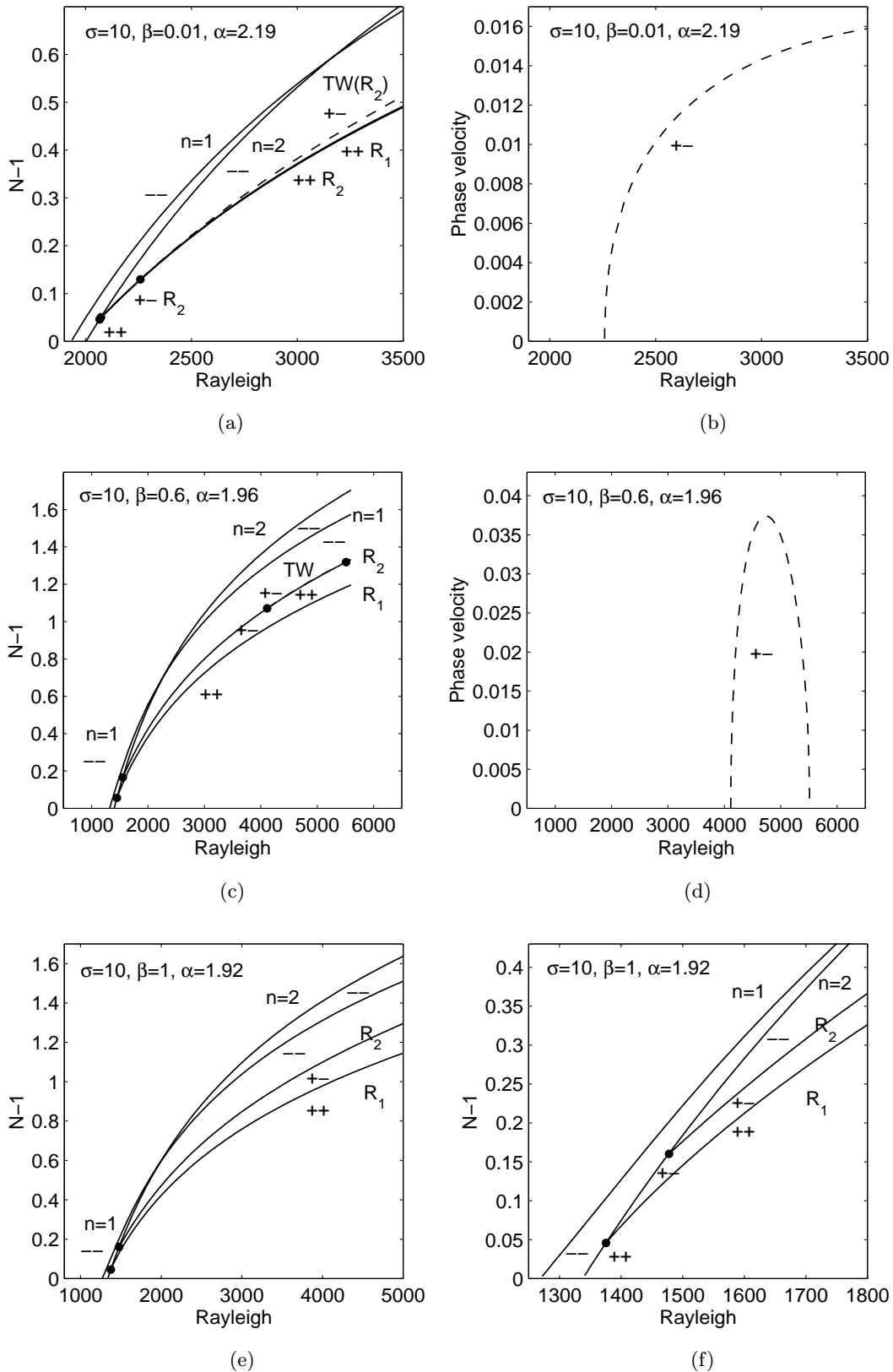


Fig. 3. Numerical results for  $\sigma = 10$  and  $\alpha > \alpha_c$ . (a) The Nusselt number  $N - 1$  and (b) the phase speed  $c$  of traveling waves as functions of  $Ra$  for  $\alpha = 2.19$ ,  $\beta = 0.01$ , for comparison with Fig. 2. (c, d) The same but for  $\alpha = 1.96$ ,  $\beta = 0.6$ . (e) The same as (c) but for  $\alpha = 1.92$ ,  $\beta = 1$ , with (f) showing a detail of (e). Note the presence of a TW “bubble” in (c) and (d). The sign of  $c$  is arbitrary since waves can travel to the left or the right.

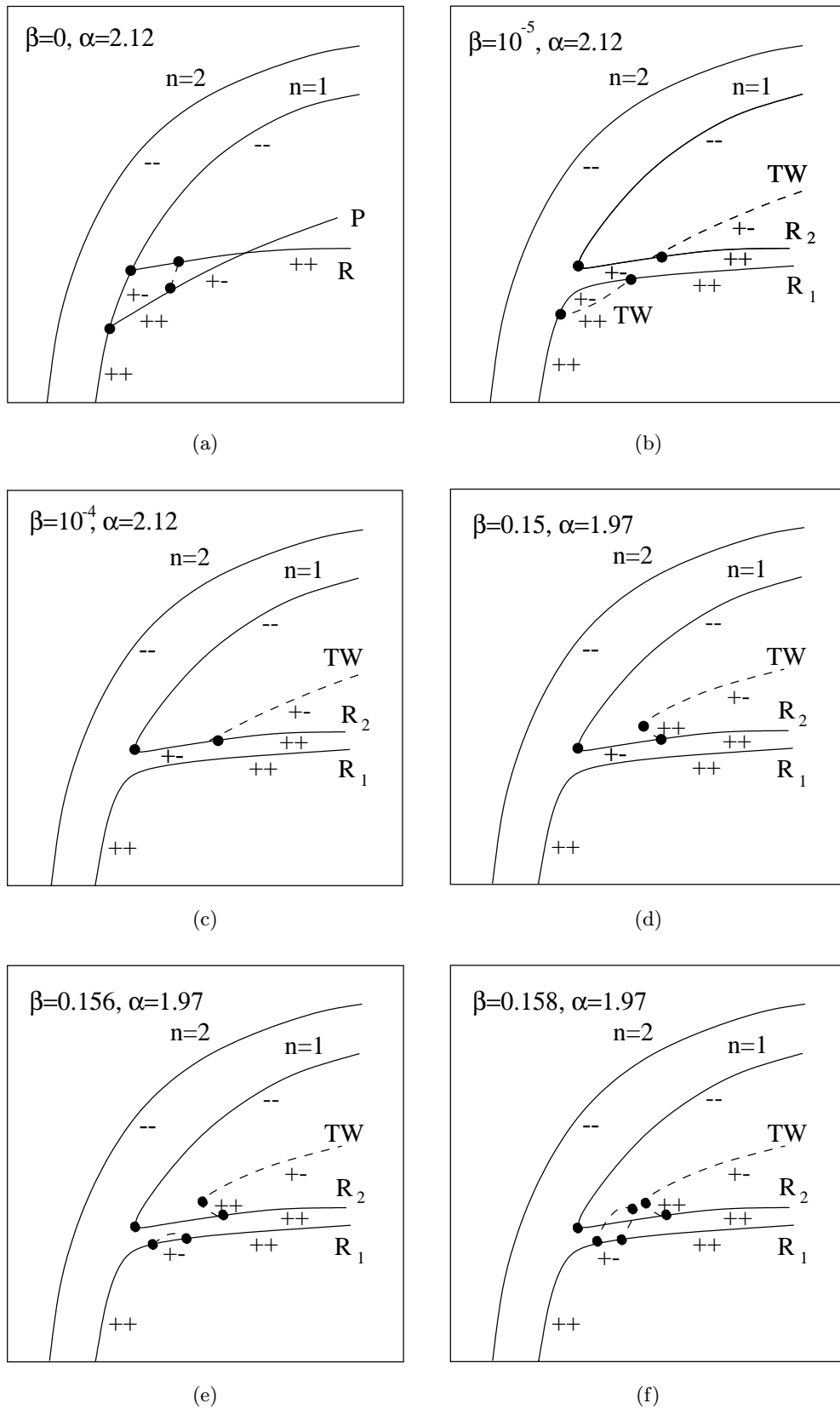


Fig. 4. Schematic bifurcation diagrams for  $\sigma = 10$  and  $\alpha < \alpha_c$ . (a)  $\alpha = 2.12, \beta = 0$ , (b)  $\alpha = 2.12, \beta = 10^{-5}$ , (c)  $\alpha = 2.12, \beta = 10^{-4}$ , (d)  $\alpha = 1.97, \beta = 0.15$ , (e)  $\alpha = 1.97, \beta = 0.156$ , (f)  $\alpha = 1.97, \beta = 0.158$ , (g)  $\alpha = 1.97, \beta = 0.16$ , and (h)  $\alpha = 1.82, \beta = 1$ . In all cases the large amplitude behavior is the same as in Fig. 3.

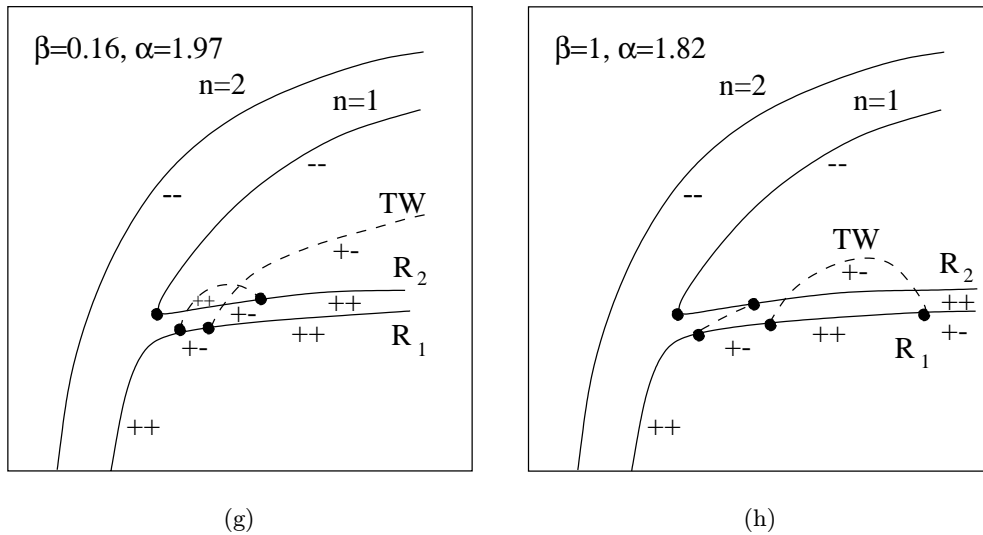


Fig. 4. (Continued)

In contrast the upper  $n = 1$  branch is an amalgam of the upper part of the original  $n = 1$  branch and the  $R_2$  branch, connected via a saddle-node bifurcation. The large amplitude TW branch produced from the  $P$  branch bifurcates below the saddle-node. Consequently the whole of the  $n = 1$  branch above the saddle-node is stable. As shown in Fig. 5(a) the phase velocity of the TW along the large amplitude branch passes through a sharp maximum. This is a consequence of the fact that the initial part of this branch was a TW branch even when  $\beta = 0$ . Consequently the drift speed along this part of the branch is necessarily substantially larger than the slow drift of the  $P$  states that form the remainder of the TW branch due to the broken midplane reflection symmetry. Note that even with  $\beta$  this small, the computed bifurcation diagram lacks the expected saddle-node bifurcation on the TW bubble that should be inherited from the break-up of the TW present when  $\beta = 0$ . This is because the  $\beta = 0$  TW branch is almost vertical.

Figure 4 shows that as  $\beta$  increases the TW bubble on the  $R_1$  branch rapidly disappears, leaving only one TW branch. This branch bifurcates supercritically from the  $R_2$  branch, as shown in Fig. 6(a) in the form of a Nusselt number versus  $Ra$  diagram computed for  $\beta = 0.01$ . However, by  $\beta = 0.15$  the TW branch has changed its direction of bifurcation from the  $R_2$  branch, and now bifurcates subcritically. Moreover, by  $\beta = 0.156$  a TW bubble reappears on the  $R_1$  branch, and develops a saddle-node bifurcation which then annihilates with the

saddle-node bifurcation on the other TW branch. This process results in a reconnection of the TW branches and produces a TW segment connecting the  $R_1$  and  $R_2$  branches, and a large amplitude TW branch that now bifurcates from the  $R_1$  branch (see Fig. 4(g) for  $\beta = 0.16$ ). This interesting bifurcation is described further in Sec. 4 and is required if one is to understand the origin of the  $\beta = 1$  bifurcation diagram [Fig. 4(h)]. As before, Fig. 5 shows the corresponding quantitative changes in the TW phase velocity. Note in particular the formation of the loop when  $\beta = 0.15$  and the “necking” accompanying the disappearance of the TW saddle-node bifurcations [Figs. 5(c)–5(f)].

Note that at larger amplitude the bifurcation diagrams for  $\beta = 0$  must be independent of whether  $\alpha > \alpha_c$  or  $\alpha < \alpha_c$ , and likewise for  $\beta = 1$ . As a result the TW branch that appears in Fig. 4 must in fact terminate at finite amplitude on one of the  $R$  branches, and cannot extend to infinite amplitude [cf. Fig. 4(h)]. Figure 6(b) shows the Nusselt number versus  $Ra$  for  $\beta = 1$ . The TW branch present in this figure in fact terminates at larger  $Ra$  back on the  $R_1$  branch, as can be seen from Fig. 5(h), and so does not extend to large amplitudes. This should come as no surprise since the large amplitude behavior for  $\alpha < \alpha_c$  and  $\alpha > \alpha_c$  must be identical.

### 3.3. The case $\sigma = 0.1$ : $\alpha > \alpha_c$

For low Prandtl numbers the situation is more complex. Figure 7 summarizes schematically the

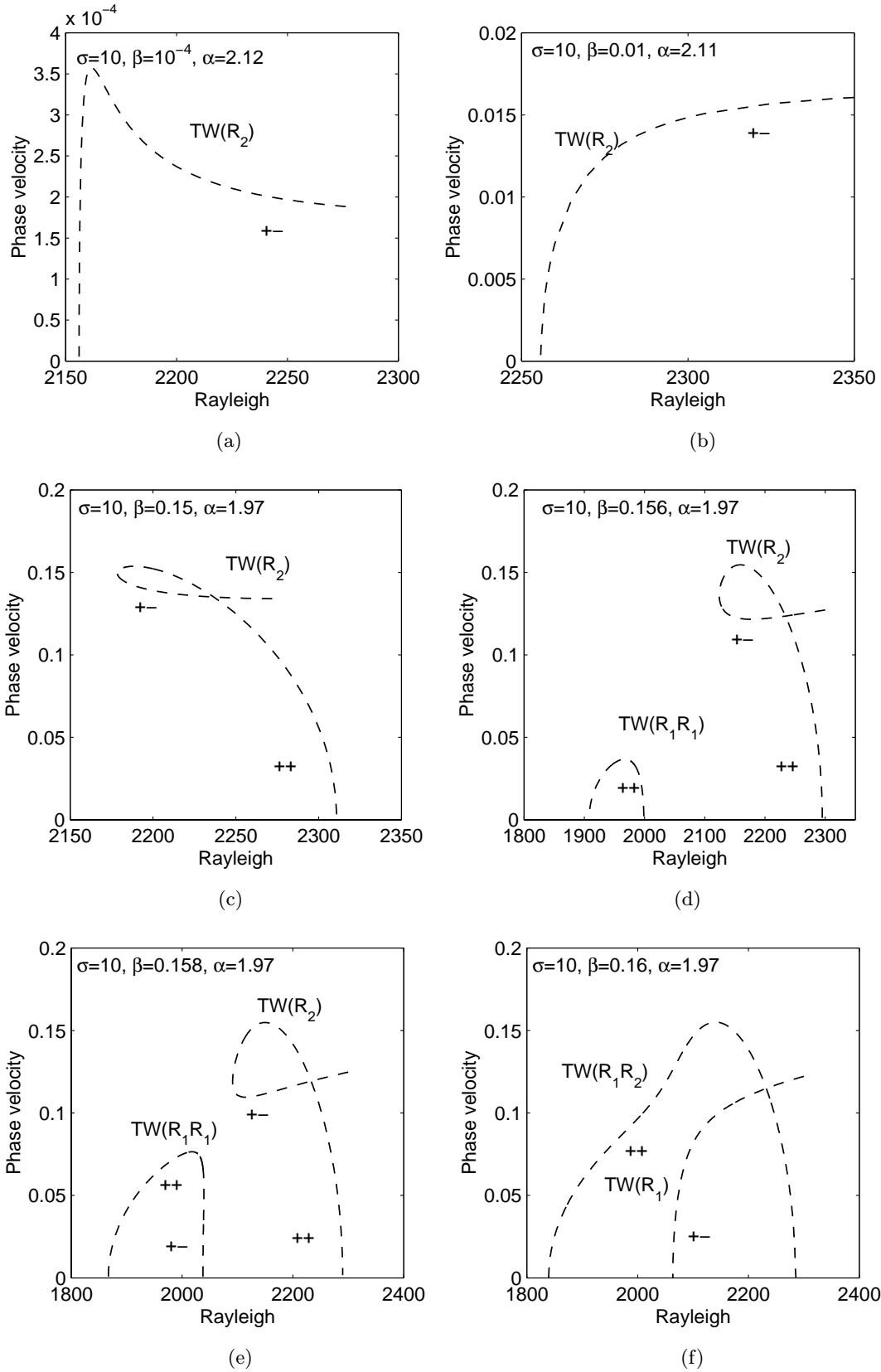


Fig. 5. Phase speed of the traveling waves in Fig. 4 computed numerically as a function of  $Ra$ : (a)  $\alpha = 2.12, \beta = 10^{-4}$ , (b)  $\alpha = 2.11, \beta = 0.01$ , (c)  $\alpha = 1.97, \beta = 0.15$ , (d)  $\alpha = 1.97, \beta = 0.156$ , (e)  $\alpha = 1.97, \beta = 0.158$ , (f)  $\alpha = 1.97, \beta = 0.16$ , (g)  $\alpha = 1.95, \beta = 0.2$ , and (h)  $\alpha = 1.82, \beta = 1$ . Note, in particular, the “necking” transition between (e) and (f).

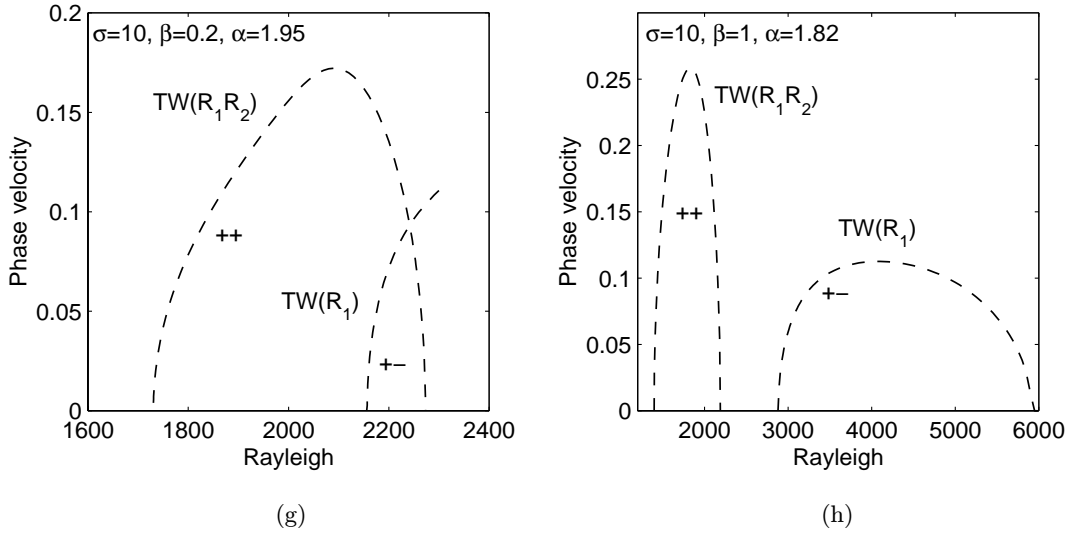


Fig. 5. (Continued)

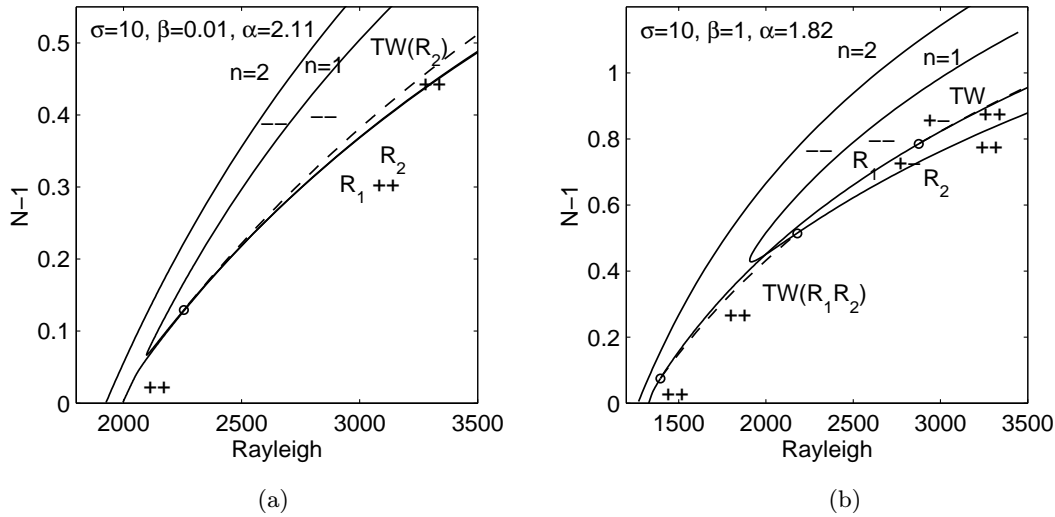


Fig. 6. The Nusselt number  $N - 1$  as a function of  $Ra$  for (a)  $\sigma = 10$ ,  $\alpha = 2.11$  and  $\beta = 0.01$ , showing the transformation of the  $R$  and  $P$  branches into  $R_{1,2}$  and  $TW(R_2)$ , respectively. (b) The results for  $\alpha = 1.82$  and  $\beta = 1$ .

results for  $\sigma = 0.1$ ,  $\alpha > \alpha_c$  and various values of  $\beta$ . When  $\beta = 0$  and  $\alpha = 2.2$  the basic features of the bifurcation diagram remain the same as for  $\sigma = 10$ ,  $\alpha > \alpha_c$ , but with two important differences. First, the  $R$  branch terminates on the  $n = 1$  branch at  $Ra = 4980$  with the  $n = 1$  branch unstable at higher Rayleigh numbers. Two branches of TW are also present. A short segment in  $2155 < Ra < 2190$  connects the  $R$  and  $P$  branches, with a second bifurcation to TW occurring on the  $P$  branch at  $Ra = 2710$ . These bifurcations are all parity-breaking bifurcations from

circles of reflection-symmetric states (i.e. from states with a symmetry that involves  $R$ ) and so generate unstable TW via steady state bifurcation.

As soon as the midplane reflection is broken ( $\beta > 0$ ) the  $P$  branch becomes a TW while the multiple bifurcation on the  $n = 2$  branch splits into two successive bifurcations to  $R$ -symmetric states as for  $\sigma = 10$ . However, the presence of the TW when  $\beta = 0$  complicates this process considerably [Mercader *et al.*, 2001a]. Figure 7 shows what happens when  $\beta = 10^{-4}$  and for successively larger values of  $\beta$ . For very small  $\beta$  the  $P$  branch

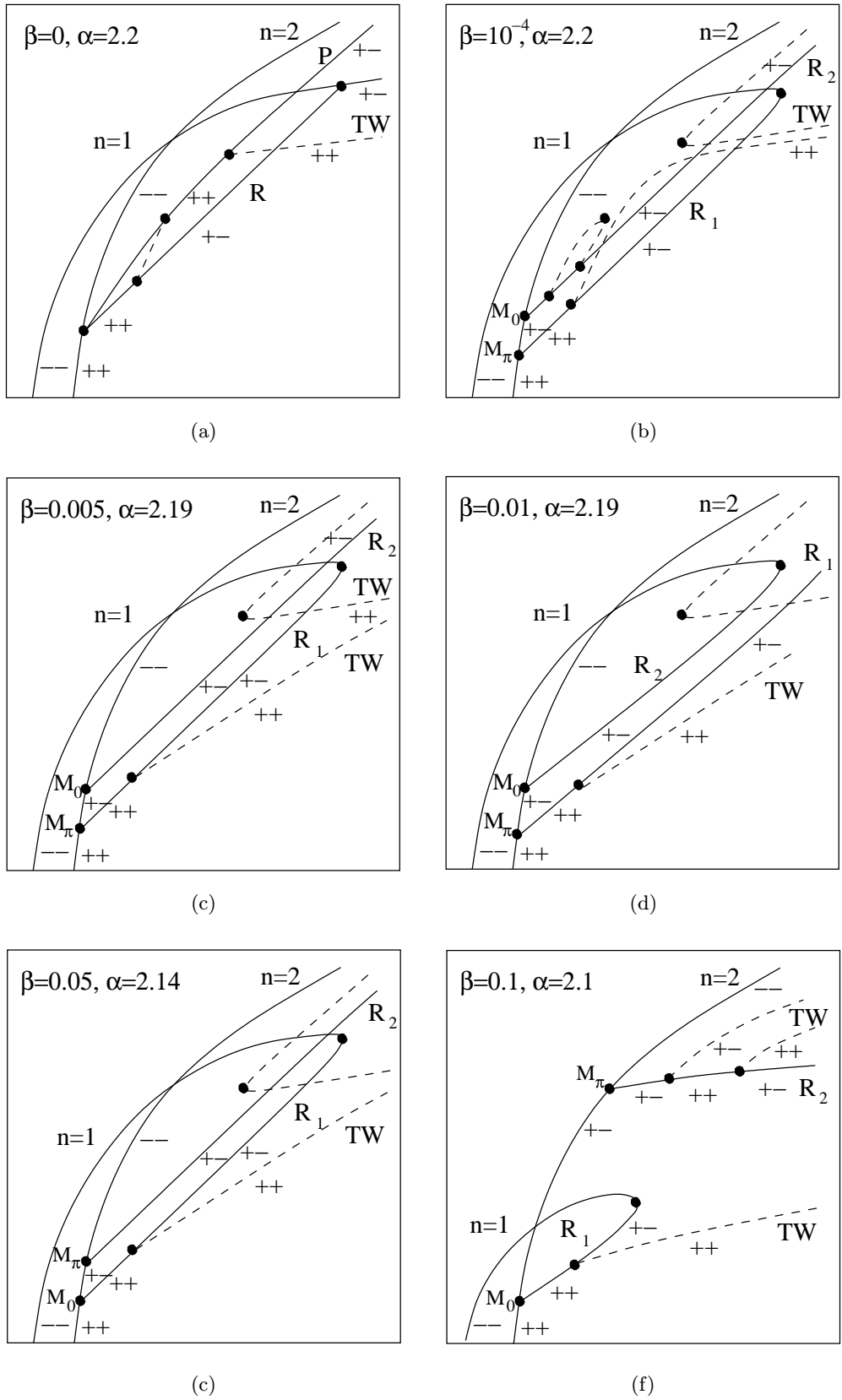


Fig. 7. Schematic bifurcation diagrams for  $\sigma = 0.1$  and  $\alpha > \alpha_c$ . (a)  $\alpha = 2.2, \beta = 0$ , (b)  $\alpha = 2.2, \beta = 10^{-4}$ , (c)  $\alpha = 2.19, \beta = 0.005$ , (d)  $\alpha = 2.19, \beta = 0.01$ , (e)  $\alpha = 2.14, \beta = 0.05$ , (f)  $\alpha = 2.1, \beta = 0.1$ , (g)  $\alpha = 2.05, \beta = 0.2$ , (h)  $\alpha = 2.0, \beta = 0.3$ . The solid (dashed) lines denote steady (traveling) solutions. Secondary bifurcations of steady (Hopf) type are indicated by solid (open) circles, and stability by the signs of the two leading eigenvalues, with + (-) indicating instability (stability).

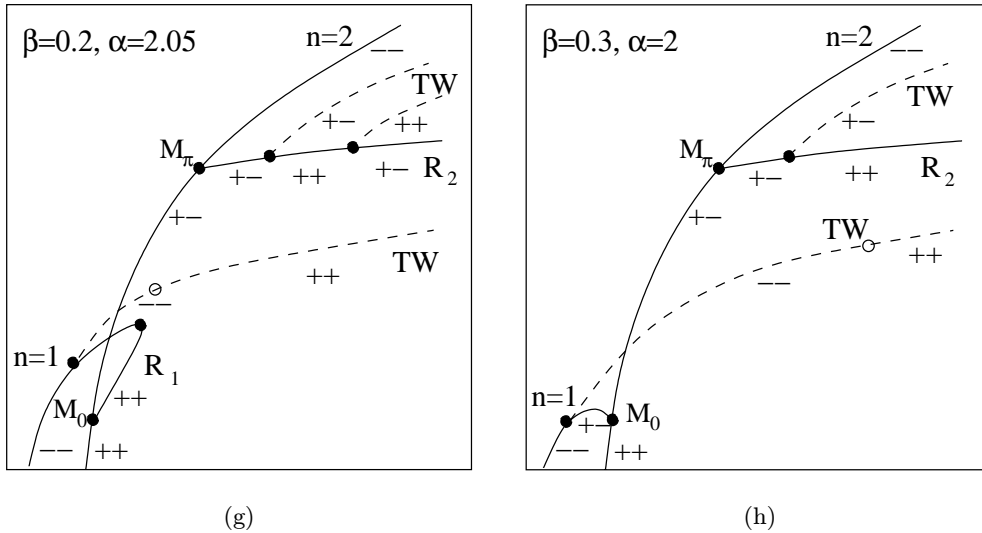


Fig. 7. (Continued)

becomes a TW branch that connects smoothly with the TW branches produced by the splitting of the original TW branches by the broken midplane reflection symmetry. As a result there is TW “bubble” on the  $R_2$  branch containing a TW saddle-node bifurcation. There is also a bifurcation to TW on the  $R_1$  branch at  $Ra = 2155$  with the resulting TW extending to large  $Ra$ , and a disconnected TW segment created via a saddle-node bifurcation. Of particular significance in what follows is the fact that the  $R_1$  branch connects smoothly to the  $n = 1$  branch. As a result the  $n = 1$  branch has only a finite extent before annihilation in a collision with the  $R_1$  branch; its role at large  $Ra$  is assumed by the  $R_2$  branch.

As  $\beta$  increases the situation rapidly simplifies. For example, by the time  $\beta$  reaches  $\beta = 0.005$  the TW bubble disappears [Fig. 7(c)], leaving only a single bifurcation to TW on the  $R_1$  branch, although with increasing  $\beta$  the disconnected TW branch eventually reconnects again with the  $R_2$  branch (see below). Then at  $\beta$  between  $\beta = 0.0093$  and  $\beta = 0.0094$  (for  $\alpha = 2.19$ ) the saddle-node on the  $n = 1$  branch collides with the  $R_2$  branch forming a pitchfork bifurcation (see Sec. 4.3), and for larger  $\beta$  the  $n = 1$  branch terminates at  $M_0$  instead of  $M_\pi$  [see Figs. 7(c) and 7(d)]. This reconnection has no effect on the relative location of the points  $M_0$  and  $M_\pi$  or on the TW bifurcation, which remains on the  $R_1$  (i.e. lower) branch. The bifurcation diagram that results is shown in Fig. 7(d) for  $\beta = 0.01$ . However, by the time  $\beta$  reaches  $\beta = 0.05$

[Fig. 7(e)] the locations of the secondary bifurcations  $M_0$  and  $M_\pi$  have traded positions, restoring the topology of the  $\beta = 0.005$  diagram but with  $M_0$  and  $M_\pi$  now reversed. The details of this transition are involved. For  $\alpha = 2.18$  we find that the exchange takes place very near  $\beta = 0.024 (= \beta_c)$  and occurs as follows. For  $\beta < \beta_c$  the branch  $R_1$  connects to  $M_\pi$  while  $R_2$  connects to  $M_0$ . Of these the  $R_1$  branch undergoes a parity-breaking bifurcation producing a branch  $TW(R_1)$  that extends to larger amplitudes [cf. Fig. 7(d)]. However, by  $\beta = 0.020$  a pair of additional parity-breaking bifurcations appears on the branch  $R_2$  producing a TW bubble with a small hysteresis at one end. The amount of hysteresis increases with  $\beta$ , and a “necking” bifurcation (Sec. 4.4) occurs between  $\beta = 0.0213$  and  $\beta = 0.0214$  (see Fig. 8). The resulting  $TW(R_2)$  now extends to larger amplitudes, leaving behind a segment  $TW(R_2R_1)$  connecting  $R_1$  with  $R_2$ . Specifically, when  $\beta = 0.022$ ,

- $R_1$  ( $M_\pi$ ) bifurcates from  $n = 2$  at  $Ra = 2001$
- $R_2$  ( $M_0$ ) bifurcates from  $n = 2$  at  $Ra = 2002.4$
- $TW(R_2)$  is born at  $Ra = 2076$
- $TW(R_2R_1)$  extends from  $Ra = 2012$  ( $R_2$ ) to 2078 ( $R_1$ ).

The value of the Rayleigh number at which the  $TW(R_2R_1)$  segment bifurcates from  $R_2$  moves towards the point  $M_0$  on the  $n = 2$  branch as  $\beta$  approaches  $\beta_c$ , and at  $\beta = \beta_c$  these two points coincide with  $M_\pi$ . For  $\beta > \beta_c$  the points  $M_0$  and  $M_\pi$  have traded positions, and the point at which the

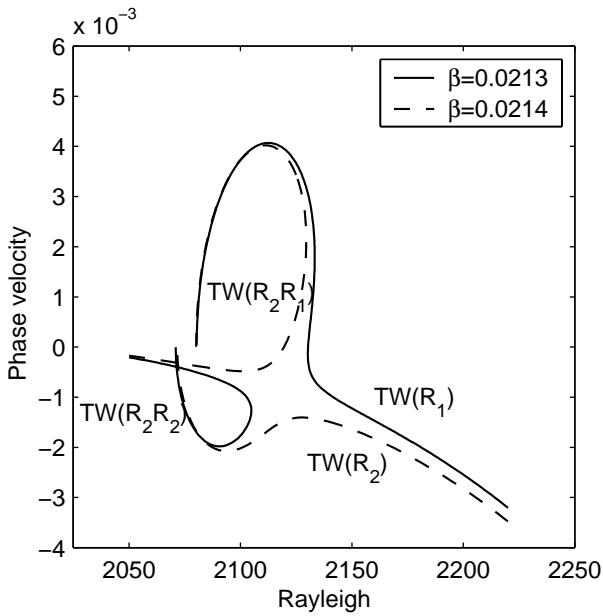


Fig. 8. The phase speed  $c$  of the TW participating in the “necking” bifurcation as a function of  $Ra$  for  $\sigma = 0.1$ ,  $\alpha = 2.18$ . The branches originating from the  $c = 0$  line appear in parity-breaking bifurcations from steady states. The “necking” bifurcation provides the key to the transition between Figs. 7(d) and 7(e), with the large  $Ra$  branch corresponding to the TW branch in these figures. See text for further discussion.

TW segment first appears reemerges on the new  $R_2$  branch, thereby forming a TW bubble on the new  $R_2$  branch. This bubble disappears with increasing  $\beta$ , leaving behind a diagram of the type

shown in Fig. 7(e). Although this transition appears to be unnecessarily complex related transitions are typical of near-degenerate steady state bifurcations with broken  $D_4$  symmetry [Crawford & Knobloch, 1988; Bergeon *et al.*, 2001], as discussed further in Sec. 4.6. After the above sequence of bifurcations the point  $M_\pi$  moves to larger amplitude as  $\beta$  increases in the interval  $0.05 < \beta < 0.1$  but thereafter remains almost stationary. When  $\beta = 0.1$  [Fig. 7(f)] the disconnected TW branch [see Fig. 7(a)] collides with the branch  $R_2$  emanating from  $M_\pi$ , producing two successive bifurcations to TW (see Sec. 4). With increasing  $\beta$  the larger amplitude bifurcation point moves off to “infinity”. At the same time the saddle-node bifurcation moves to smaller amplitude, opening up an interval in Rayleigh number containing no simple stable states. This interval grows with  $\beta$  as the TW bifurcation on the  $n = 1$  branch moves past the saddle-node bifurcation, decreasing the range of stable  $n = 1$  states. Figures 9(a) and 9(b) show that when  $\beta = 0.2$  the “gap” in  $Ra$  extends from  $Ra = 1710$  to  $Ra = 2410$ . We anticipate that in this range of  $Ra$  complex dynamics will be present, since the motion of the bifurcation to TW past the saddle-node creates a tertiary Hopf bifurcation on the TW branch (see Sec. 4) that produces quasiperiodic (i.e. two-frequency) traveling waves [Mercader *et al.*, 2001b]. However, by  $\beta = 0.3$  the tertiary Hopf bifurcation has moved to large values of  $Ra$ ,

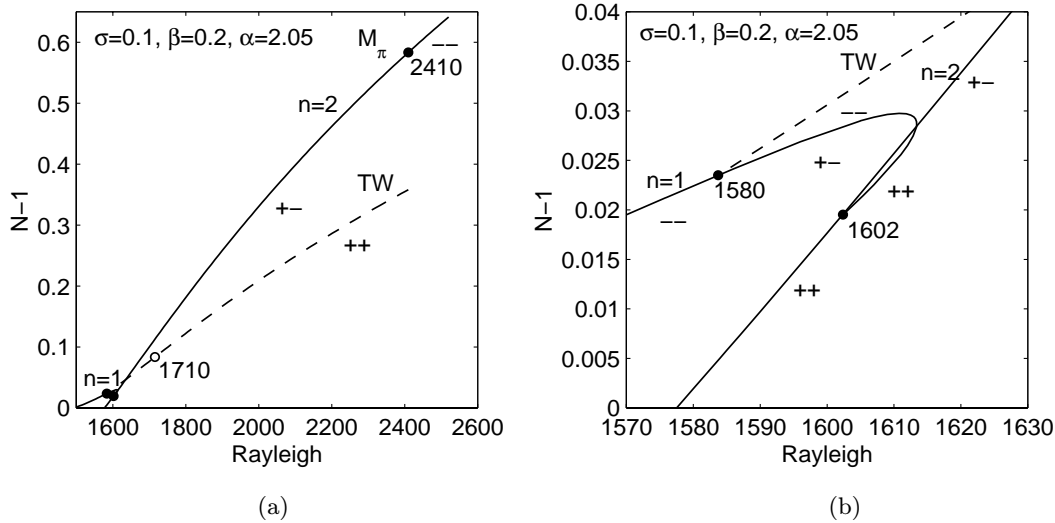


Fig. 9. The Nusselt number  $N - 1$  as a function of  $Ra$  for  $\sigma = 0.1$ , (a, b)  $\alpha = 2.05$  and  $\beta = 0.2$ , and (c, d)  $\alpha = 2.0$  and  $\beta = 0.3$ , showing the rapid increase in stability of the TW branch with increasing  $\beta$ . Note especially the presence of the “gap”,  $1710 < Ra < 2410$ , in (a) in which there are no simple stable solutions; this gap is completely absent in (c). (b, d) show details of (a, c), respectively.

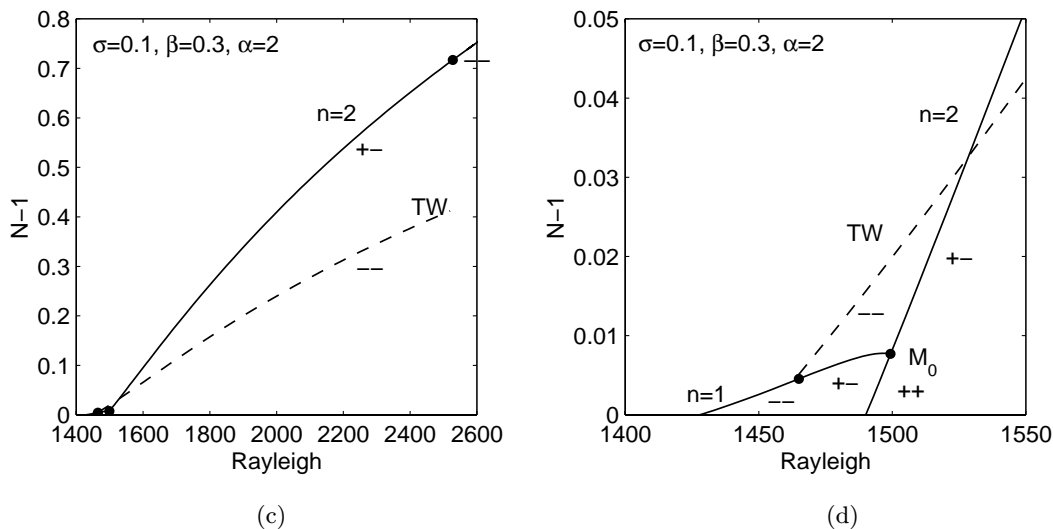


Fig. 9. (Continued)

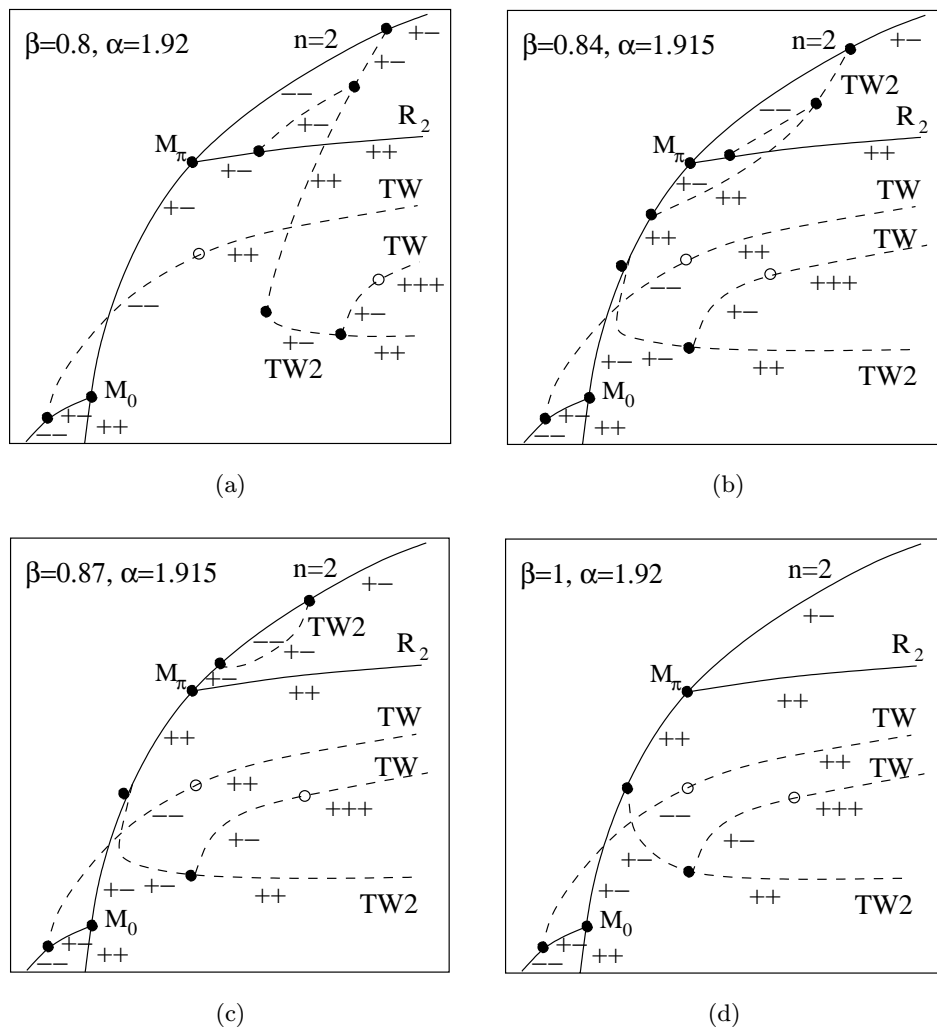


Fig. 10. Schematic bifurcation diagrams for  $\sigma = 0.1$  and  $\alpha > \alpha_c$  (continued). (a)  $\alpha = 1.92$ ,  $\beta = 0.8$ , (b)  $\alpha = 1.915$ ,  $\beta = 0.84$ , (c)  $\alpha = 1.915$ ,  $\beta = 0.87$ , (d)  $\alpha = 1.92$ ,  $\beta = 1$ . The solid (dashed) lines denote steady (traveling) solutions. Secondary bifurcations of steady (Hopf) type are indicated by solid (open) circles, and stability by the signs of the two leading eigenvalues, with + (-) indicating instability (stability).

leaving behind stable TW and closing the gap [Figs. 9(c) and 9(d)]. The saddle-node bifurcation on the  $n = 1$  branch then disappears as well, as shown in Fig. 7(h) for  $\beta = 0.3$ . As shown in Fig. 10, for larger values of  $\beta$  all the action takes place at larger amplitudes, and is associated with the approach of a TW bifurcation along the  $n = 2$  branch from large amplitude to smaller that destabilizes the large amplitude  $n = 2$  states. We refer to the resulting TW branch as TW2 to indicate that these TW bifurcate from the pure mode branch  $n = 2$  (i.e. the TW2 have no odd wavenumber components), in contrast to the TW encountered hitherto which bifurcated from the mixed mode branch

$R_2$  and contain contributions from all wavenumbers. Note that the TW2 branch is strongly subcritical; consequently its presence limits dramatically the region of stability of simple and computable large amplitude states. This occurs via a complex sequence of bifurcations as we now describe. Observe first [see Fig. 10(a)] that the TW branch that bifurcates from the  $R_2$  branch terminates on the TW2 branch in a steady state subharmonic bifurcation; the details of this bifurcation are also discussed in Sec. 4. A similar bifurcation occurs further along the TW2 branch and produces a branch called TW possessing a Hopf bifurcation, whose presence is probably related to the proximity to a saddle-node

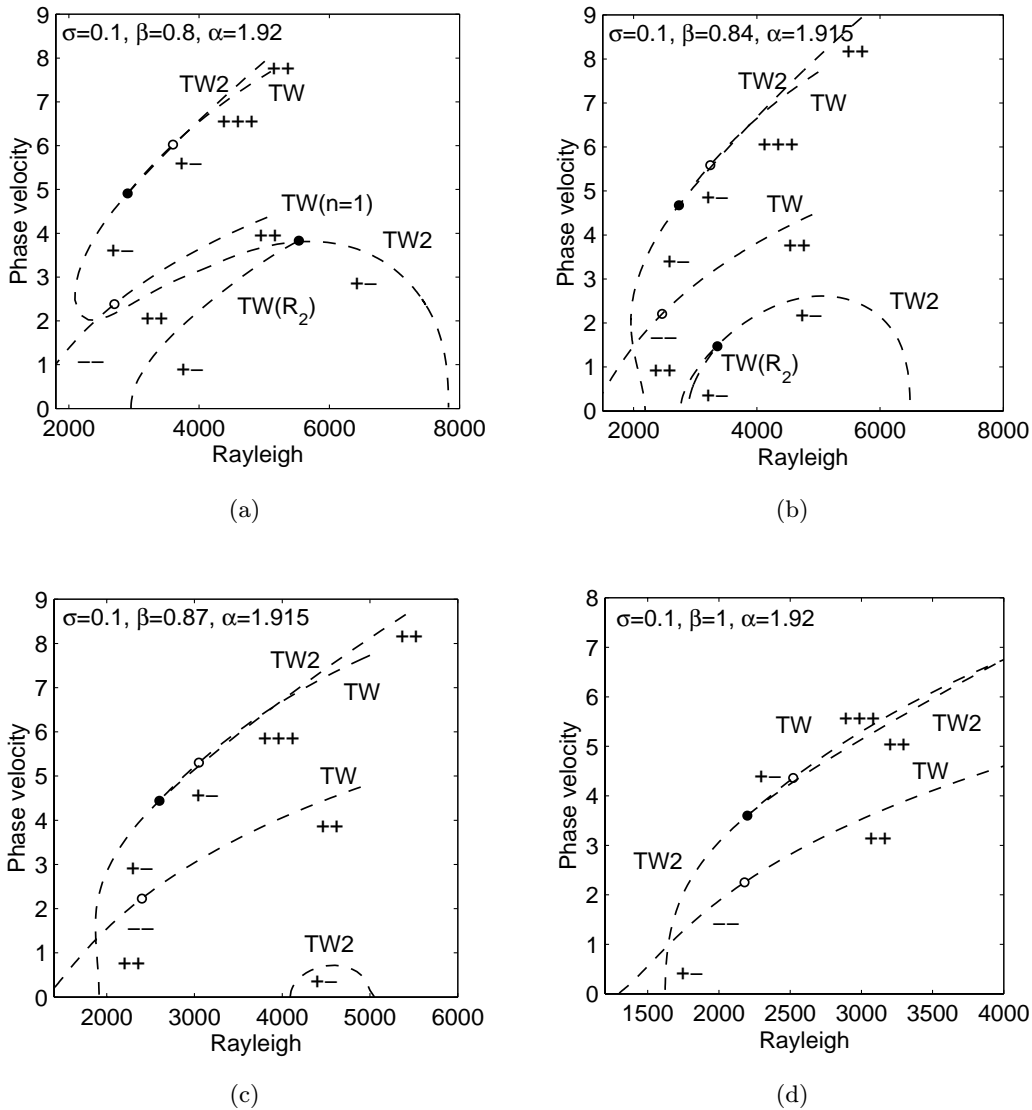


Fig. 11. Phase velocity for the traveling waves in Fig. 10 as a function of  $Ra$ . (a)  $\alpha = 1.92, \beta = 0.8$ , (b)  $\alpha = 1.915, \beta = 0.84$ , (c)  $\alpha = 1.915, \beta = 0.87$ , (d)  $\alpha = 1.92, \beta = 1$ . The points where  $c = 0$  represent parity-breaking bifurcations from (circles of) steady states. The label TW2 indicates waves lacking odd wavenumbers. Solid (open) circles indicate steady (Hopf) bifurcations.

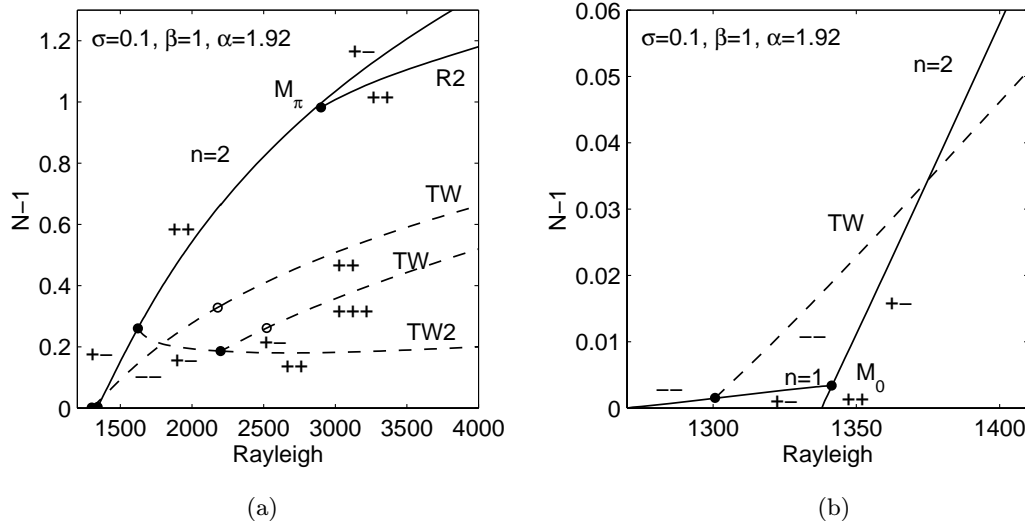


Fig. 12. The Nusselt number  $N - 1$  as a function of  $Ra$  for  $\sigma = 0.1$ ,  $\alpha = 1.92$  and  $\beta = 1$ , showing that all simple solutions are unstable for  $Ra > 2195$ . (b) Shows a detail of (a). Solid (open) circles indicate steady (Hopf) bifurcations.

bifurcation on the TW2 branch [see Fig. 10(a)]. The TW2 branch then becomes tangent to the  $n = 2$  branch, producing two additional bifurcations to TW2 on this branch. The upper of these moves towards larger amplitude past the point  $M_\pi$  [Figs. 10(b) and 10(c)], annihilating in the process the branch TW that bifurcates from  $R_2$  and leaving only a TW2 bubble at large amplitude. These transitions are summarized in Fig. 11, where the phase velocity of the traveling waves is shown as a function of  $Ra$ . With increasing  $\beta$  this TW2 bubble disappears [Fig. 11(c)], leaving the  $\beta = 1$  diagram shown in Fig. 10(d); the corresponding Nusselt number diagram is shown in Fig. 12. This diagram, like the earlier ones for smaller  $\beta$ , is of interest since for  $Ra > 2195$  none of the simple states we compute remains stable. From the calculations performed the only likely stable state in this regime is the quasiperiodic (i.e. two-frequency) state that bifurcates from TW at  $Ra \approx 2195$ , with the (new) frequency  $\omega_2 \approx 4.04$ . The interesting dynamics that results requires direct numerical simulation, and is explored elsewhere [Mercader *et al.*, 2001b].

### 3.4. The case $\sigma = 0.1$ : $\alpha < \alpha_c$

When  $\alpha < \alpha_c$  the situation is almost as complicated. Figure 13(a) shows that when  $\beta = 0$  and  $\alpha = 2.12$  the  $n = 2$  branch bifurcates first and is stable throughout. The  $n = 1$  branch is also supercritical but is unstable, with a secondary bifurcation to an unstable  $P$  branch at  $Ra = 2150$ ,

followed by a tertiary bifurcation to unstable TW at  $Ra = 3220$ . Once again this is a parity-breaking bifurcation from a circle of  $P$  states. The absence of an  $R$  branch is particularly noteworthy, since the  $n = 1$  branch now remains unstable, eliminating the possibility of bistability between the  $n = 1$  and  $n = 2$  branches. When  $\beta = 10^{-4}$  the diagram breaks up in an obvious way [see Fig. 13(b)]: the  $P$  branch becomes a TW and the original TW splits into two, labeled  $TW_1$  and  $TW_2$ , forming a branch of traveling waves that extends from a bifurcation on the  $n = 1$  branch to large amplitudes, and a disconnected traveling wave branch formed from what was the large amplitude  $P$  branch and  $TW_2$ . As a result the former branch is composed of an initial part that is a drifting  $P$  state and hence is characterized by a relatively small value of  $c$ , followed by  $TW_1$  at larger values of  $Ra$ , i.e. a part that was a TW even in the  $\beta = 0$  system, and hence is characterized by a substantially larger phase velocity, cf. [Mercader *et al.*, 2001a]. For the same reason we expect the phase velocity along the latter branch to drop dramatically near the saddle-node bifurcation as one traverses the disconnected branch towards larger amplitudes.

When  $\beta = 0.14$  and  $\alpha = 1.99$  the  $n = 1$  branch develops a hysteresis bifurcation below the bifurcation to TW [Figs. 14(a) and 14(b)]; the latter moves to lower amplitudes with increasing  $\beta$  and interacts with the saddle-node bifurcations created in the hysteresis bifurcation. However, as discussed in Sec. 4, this interaction is complicated by the

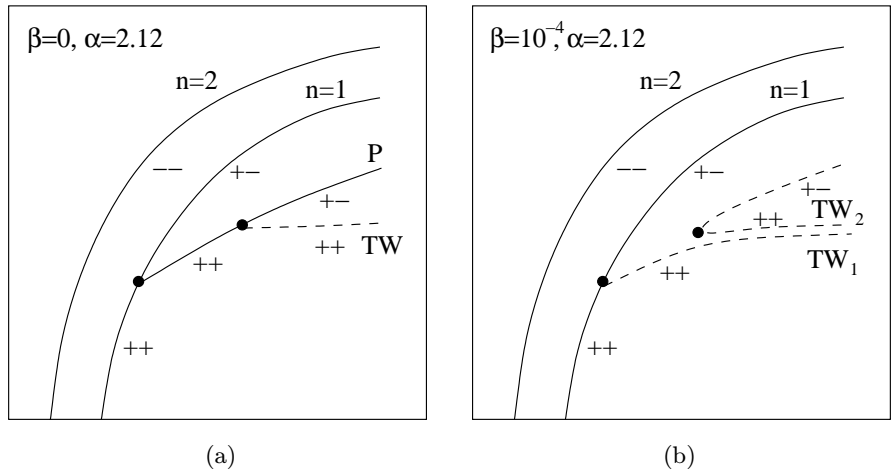


Fig. 13. Schematic bifurcation diagrams for  $\sigma = 0.1$  and  $\alpha < \alpha_c$ . (a)  $\alpha = 2.12$ ,  $\beta = 0$ , (b)  $\alpha = 2.12$ ,  $\beta = 10^{-4}$ , showing the breakup of the pitchfork to TW in (a) when  $\beta$  becomes nonzero.

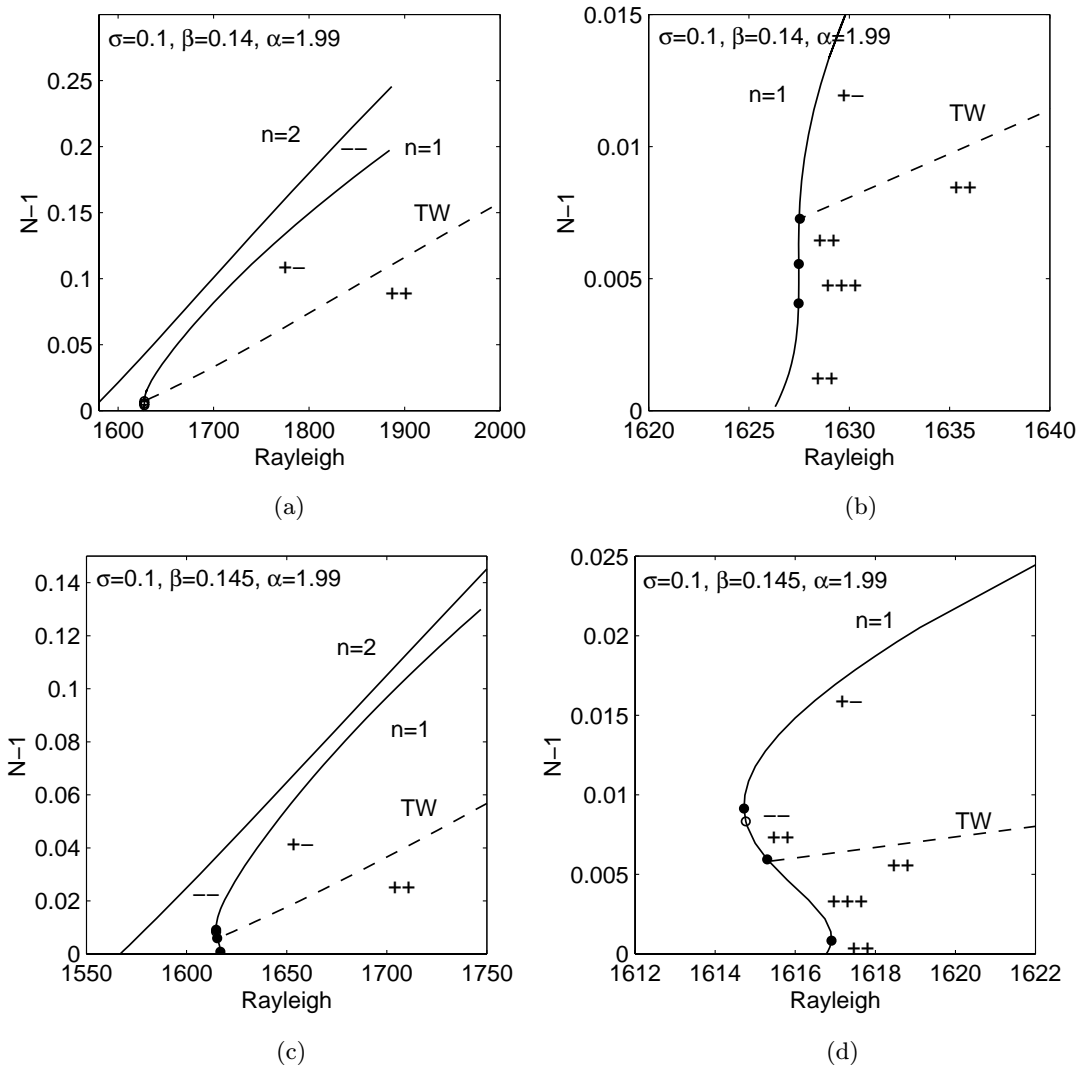
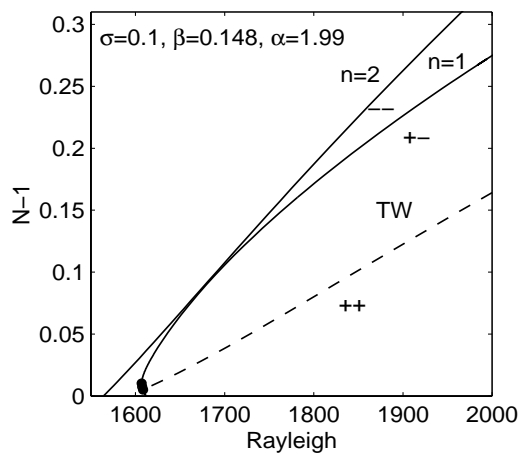
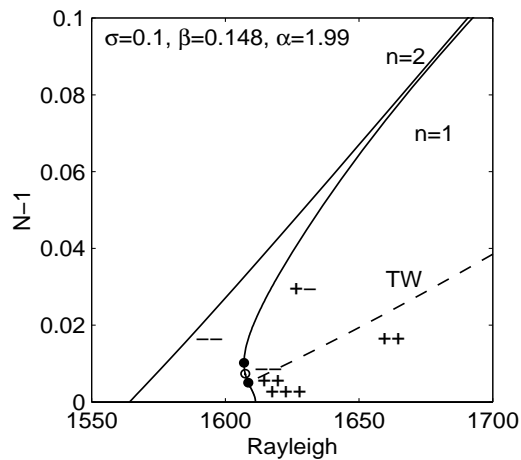


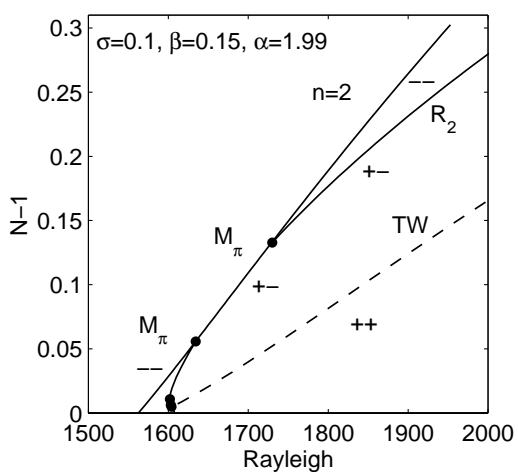
Fig. 14. The Nusselt number  $N - 1$  as a function of  $Ra$  for  $\sigma = 0.1$  and  $\alpha = 1.99 < \alpha_c$ . (a, b)  $\beta = 0.14$ , (c, d)  $\beta = 0.145$ , (e, f)  $\beta = 0.148$ , (g, h)  $\beta = 0.15$ , showing the behavior on either side of the saddle-node pitchfork bifurcation, and the appearance of the Hopf bifurcation to standing waves (SW). (i, j)  $\alpha = 1.97$ ,  $\beta = 0.2$ . The second figure of each pair shows a detail of the first.



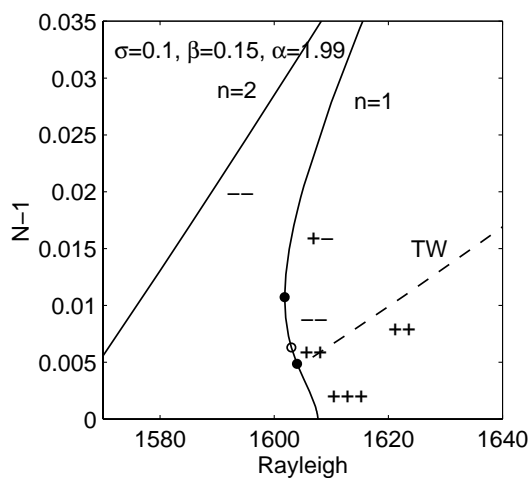
(e)



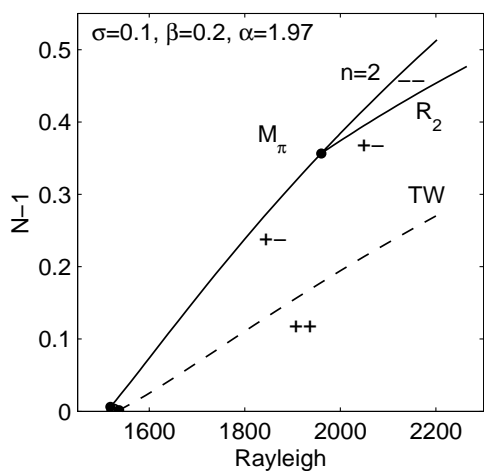
(f)



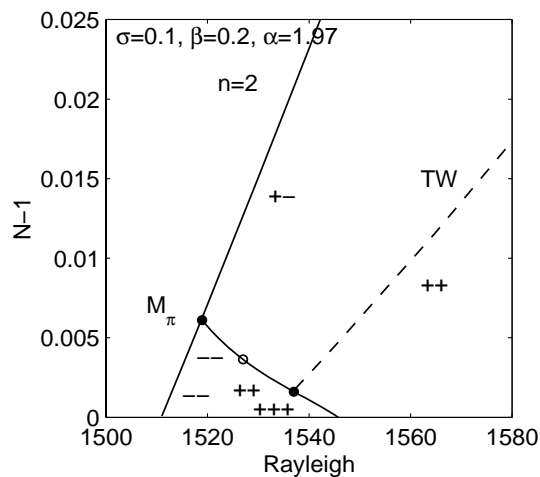
(g)



(h)



(i)



(j)

Fig. 14. (Continued)



and observe that

$$R(a_1, a_2) = (a_1, -a_2), \quad \rho(a_1, a_2) = (a_2, -a_1). \quad (5)$$

Thus [Crawford & Knobloch, 1991]

$$\dot{a}_1 = g(\lambda, a_1^2, a_2^2)a_1, \quad \dot{a}_2 = g(\lambda, a_2^2, a_1^2)a_2, \quad (6)$$

where  $g$  is a  $C^\infty$  real-valued function and  $\lambda$  denotes the distance from the bifurcation point. In the generic case these equations have only two types (modulo symmetry-related states) of nontrivial solutions near the origin (i.e. near the  $n = 2$  state). These are the states  $(a_1, a_2) = (a, 0)$  with symmetry  $R$  and the states  $(a_1, a_2) = (a, a)$  with symmetry  $R\rho$ . Observe that the solution  $(a_1, a_2) = (0, a)$  has the symmetry  $R\rho^2$  and is related to  $(a, 0)$  by  $\rho(0, a) = (a, 0)$ , and that the state  $(a, a)$  is point-symmetric. According to the above theory both the  $R$ - and the  $P$ -symmetric states bifurcate simultaneously from the  $n = 2$  state at  $\lambda = 0$ , in agreement with Fig. 2(a).

As soon as  $\beta$  becomes nonzero the symmetry of the  $n = 2$  state changes from  $D_4$  to  $D_2$ . This is because the operation  $\rho$  ceases to be a symmetry of the problem, although  $\rho^2$  remains a symmetry. As a result the secondary bifurcation splits into two successive simple bifurcations; since the symmetry  $R$  is preserved both of these produce reflection-symmetric states, one with the symmetry  $R$  and the other with the symmetry  $R\rho^2$ . The  $R$ -symmetric state is  $(a_1, 0)$  and bifurcates from the  $n = 2$  branch at the point  $M_0$ ; the  $R\rho^2$ -symmetric state  $(0, a_2)$  bifurcates instead from  $M_\pi$  (for consistency with the definitions in [Mercader *et al.*, 2001a] we need to identify the point  $M_{-\pi}$  with  $M_\pi$ ). The analogue of the  $P$  branch now branches off one of the  $R$  branches in a tertiary bifurcation; this is a consequence of the fact that this state has no remaining reflection symmetry and so cannot bifurcate from the  $n = 2$  branch; moreover, the absence of a reflection symmetry implies that this state will in fact drift along the group orbit, i.e. it will take the form of a traveling wave. We describe this process with the (truncated) normal form equations [van Gils & Mallet-Paret, 1986]

$$\begin{aligned} \dot{a}_1 &= (\lambda + \varepsilon + Aa_2^2 + B(a_1^2 + a_2^2))a_1, \\ \dot{a}_2 &= (\lambda + Aa_1^2 + B(a_1^2 + a_2^2))a_2. \end{aligned} \quad (7)$$

Here  $\varepsilon > 0$  is proportional to  $\beta$ . When  $\varepsilon = 0$  (i.e. in the  $D_4$ -symmetric case) the bifurcation diagram of

Fig. 2(a) corresponds to the choice  $A > 0$ ,  $B > 0$ ,  $A + 2B > 0$ , with  $\lambda$  proportional to  $-(Ra - Ra_c)$ . For  $\varepsilon > 0$  as  $\lambda$  increases ( $Ra$  decreases) one first encounters (at  $\lambda = -\varepsilon$ ) a subcritical bifurcation to the state  $(a, 0)$  from which there is a further bifurcation to a once unstable state of the form  $(a_1, a_2)$ ; as already mentioned, when  $\varepsilon \ll 1$  this state is almost  $P$ -symmetric and its phase velocity is proportional to  $\varepsilon$  and hence to  $\beta$ . As  $\lambda$  increases the bifurcation to  $(a_1, 0)$  from the  $n = 2$  state is followed (at  $\lambda = 0$ ) by a second subcritical bifurcation, this time to the state  $(0, a_2)$ . These predictions of Eqs. (7) and the corresponding stability assignments are completely consistent with Fig. 2(b).

Note that the normal form (7) also describes the secondary bifurcation from the  $n = 1$  branch, albeit not rigorously. This branch has symmetry  $D_2$  generated by the operations  $R$  and  $T_{L/2\kappa}$ . In appropriate variables this group acts by

$$\begin{aligned} R(a_1, a_2) &= (a_1, -a_2), \\ T_{L/2\kappa}(a_1, a_2) &= (-a_1, -a_2), \end{aligned} \quad (8)$$

so that the amplitude  $a_1$  refers to the amplitude of the  $R$ -symmetric perturbation and  $a_2$  is the amplitude of the  $P$ -symmetric perturbation (recall that  $P = RT_{L/2\kappa}$ ). Standard theory now shows that we should expect successive bifurcations to branches of solutions invariant under  $R$  and  $P$ , and this is borne out by the analysis of equations of the form (7), albeit with different interpretation of the solutions. In particular the two solutions that bifurcate from the origin now correspond to the (secondary) branches of  $R$ - and  $P$ -symmetric states seen in Fig. 4(a). Note that unless  $\varepsilon$  in Eqs. (7) is small we do not expect to see (locally) any further bifurcations from either of these branches, although such bifurcations are in fact present in Fig. 4(a).

## 4.2. Parity-breaking bifurcation

We use the term parity-breaking bifurcation to refer to a symmetry-breaking bifurcation from a circle of nontrivial equilibria. In the present problem the imposition of periodic boundary conditions together with the symmetry  $R$  of the governing equations (and boundary conditions) introduces the group  $O(2)$  of rotations and reflections of a circle into the system. As a result the primary states are all symmetric with respect to  $R$  and occur in one-parameter families, corresponding to the pattern and all its translates. Secondary bifurcations

that break the symmetry  $R$  result in drift along the group orbit, i.e. in patterns that drift horizontally, as described by the normal form

$$\dot{c} = (\lambda - c^2)c, \quad \dot{\phi} = c. \quad (9)$$

Here  $\phi$  denotes the spatial phase of the pattern, i.e.  $\chi' = \chi'(x + \phi)$  relative to some origin. Thus states with  $c = 0$  correspond to stationary (i.e. reflection-symmetric states) while those with  $c \neq 0$  represent TW. Note that these states can drift in either direction, depending on initial conditions. In the above normal form the bifurcation to TW is supercritical and the resulting TW will therefore be stable (if the primary state from which it bifurcates is stable). This type of supercritical parity-breaking bifurcation from the  $R_2$  branch can be seen, for example, in Figs. 2(b) and 2(c). Other examples can be seen in Figs. 4(b), 7(a), 7(b), etc.

The TW bubbles encountered in Sec. 3 [Fig. 3(d)] are described similarly. The normal form is

$$\dot{c} = (\varepsilon - \lambda^2 - c^2)c, \quad \dot{\phi} = c. \quad (10)$$

Thus if  $\varepsilon > 0$  a TW bubble exists in the interval  $-\varepsilon^{1/2} < \lambda < \varepsilon^{1/2}$ , and the bubble disappears as  $\varepsilon \rightarrow 0$  [Figs. 2(c) and 2(d)]. See Figs. 4(b), 4(c), 7(b), 7(c), 10(c) and 10(d) for other examples.

### 4.3. The imperfect bifurcation

There are a number of instances where an imperfect bifurcation is observed. The simplest example occurs when  $\sigma = 10$ ,  $\alpha = 2.12$  and  $\beta$  is changed from zero [Figs. 4(a) and 4(b)]. When  $\beta = 0$  the bifurcation from the  $n = 1$  branch to the  $R$  branch is a pitchfork because it breaks the symmetry  $T_{L/2}\kappa$  [see Eq. (8)]; the resulting solutions are related by  $T_{L/2}\kappa$ , and this is the reason the bifurcation diagram in Fig. 4(a) does not look like a pitchfork. However, once  $\beta$  becomes nonzero this symmetry is no longer present, and the pitchfork becomes an imperfect bifurcation. This bifurcation is described by the normal form

$$\dot{z} = \varepsilon + (-\lambda + z^2)z, \quad (11)$$

where  $z$  measures the amplitude of the  $n = 2$  contribution that enters at  $\lambda = 0$  ( $\lambda \propto (Ra - Ra_c)/Ra_c$ ), and  $\varepsilon$  is proportional to  $\beta$ . This normal form is the appropriate unfolding since we are only varying a single parameter to break the symmetry  $T_{L/2}\kappa$ . It is for this reason that we do not expect to encounter all the diagrams present in the *universal*

unfolding of the pitchfork [Golubitsky & Schaeffer, 1988], given (up to time reversal) by

$$\dot{z} = \varepsilon_1 + \varepsilon_2 z^2 + (\lambda - z^2)z.$$

Note that since  $\varepsilon$  breaks the  $T_{L/2}\kappa$  symmetry the  $R$  branch is now split into two distinct branches unrelated by symmetry, as in Fig. 4(b).

A different but very important example of an imperfect pitchfork bifurcation is provided by the transition between Figs. 7(c) and 7(d). Figure 16 shows what happens. In Fig. 16(a) we show the Nusselt number  $N - 1$  as a function of  $Ra$  when  $\beta = 0.0093$ ,  $\alpha = 2.19$  for comparison with Fig. 7(c). Evidently, the two branches are to be identified with the  $R_1$  (nonmonotonic) and  $R_2$  (monotonic) branches in Fig. 7(c). These results are presented in a more revealing form in Fig. 16(b) which shows the amplitude  $T_{00}$  of the zero temperature mode [see Eq. (4c)] along the two interacting branches, with the label  $n = 1$  indicating the branch that corresponds to the  $n = 1$  primary branch. The figure shows the situation both before (continuous line) and after (dashed line) the formation of a pitchfork bifurcation. Since the orientation of the imperfect bifurcation is reversed for  $\beta = 0.0094$  the branch  $R_1$  now corresponds to the monotonic branch and  $R_2$  to the nonmonotonic one. These figures provide strong evidence that the transition from Fig. 7(c) to Fig. 7(d) occurs via the formation of a pitchfork bifurcation at a particular value of  $\beta$ ,  $0.0093 < \beta_c < 0.0094$ , and its transformation into an imperfect bifurcation for both  $\beta < \beta_c$  and  $\beta > \beta_c$ . Note that a pitchfork bifurcation of this type forms only because the coefficient of the quadratic term in the normal form passes through zero, and not as the result of any reflection symmetry. The connection between this situation and the normal form (11) is provided by the universal unfolding just mentioned.

Other examples of imperfect bifurcations are seen, for example, in the diagrams corresponding to  $\sigma = 0.1$ ,  $\alpha = 2.12$  [Figs. 13(a) and 13(b)], where the pitchfork from the  $P$  branch to the TW branch becomes imperfect once  $\beta$  becomes nonzero (this bifurcation is described by Eq. (11) with  $z$  replaced by the phase velocity  $c$ ), and in the diagrams for  $\sigma = 0.1$ ,  $\alpha = 2.2$  [Figs. 7(a) and 7(b)], where the termination of the  $R$  branch on the  $n = 1$  branch also becomes an imperfect bifurcation. In the latter case, described by the normal form  $\dot{z} = \varepsilon + (\lambda + z^2)z$ , this bifurcation changes dramatically the overall topology of the  $n = 1$  branch.

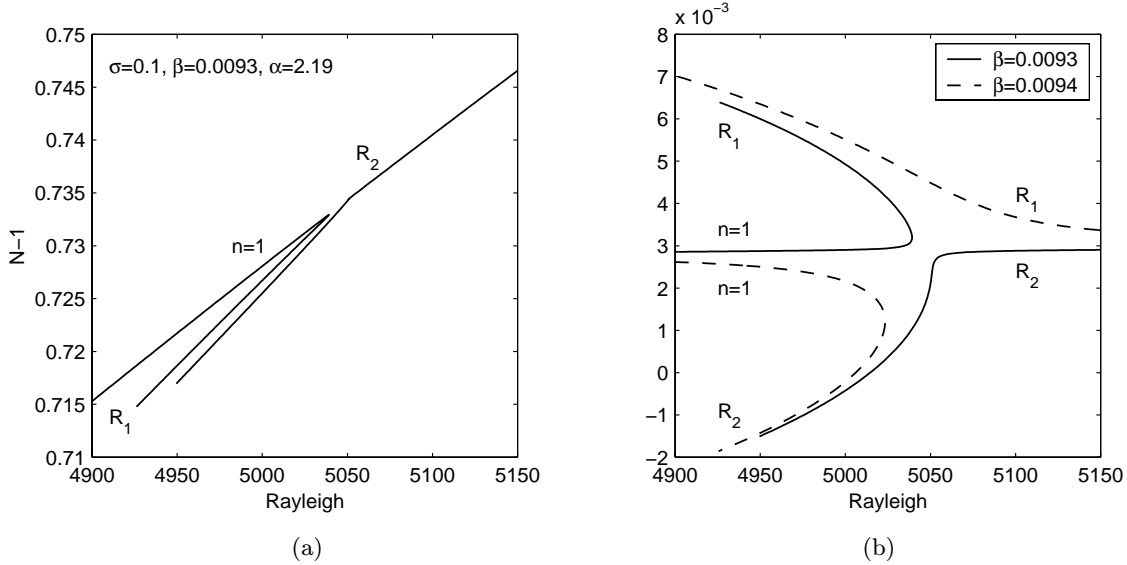


Fig. 16. (a) The Nusselt number  $N - 1$  as a function of  $Ra$  when  $\beta = 0.0093 < \beta_c$  and  $\sigma = 0.1$ ,  $\alpha = 2.19$  for comparison with Fig. 7(c). (b) The unfolding of the codimension-two pitchfork bifurcation at  $\beta = \beta_c$  when  $\beta < \beta_c$  (continuous lines) and  $\beta > \beta_c$  (broken lines), shown in terms of the temperature mode  $T_{00}$  along the two branches. The label  $n = 1$  indicates the branch that connects to the  $n = 1$  primary bifurcation.

The situation is different for the bifurcation from the  $n = 1$  branch to the  $P$  states [see Figs. 4(a) and 4(b)]. This bifurcation is also a pitchfork, but it remains a pitchfork even when  $\beta$  becomes nonzero. This is because this time the bifurcation breaks the symmetry  $R$  and this symmetry is unaffected by the loss of midplane reflection symmetry. However, due to the loss of the  $T_{L/2}\kappa$  symmetry the  $P$  states turn into TW, as already explained.

#### 4.4. The necking bifurcation

In the case  $\sigma = 10$  we encountered an instance of two branches of TW reconnecting as the parameter  $\beta$  increased [Figs. 4(f) and 4(g), 5(e) and 5(f)]. This is a standard bifurcation, and is described by the normal form

$$\dot{c} = \lambda^2 + \beta - \beta_c - c^2, \quad \dot{\phi} = c. \quad (12)$$

Here  $\beta = \beta_c$  is the location of the reconnection; at this value of  $\beta$  the normal form (12) describes a pair of straight lines intersecting at the origin. If  $\beta < \beta_c$  these break up leaving a gap in the values of  $\lambda$  for which solutions exist, while if  $\beta > \beta_c$  the straight lines reconnect in the opposite sense leaving a gap in  $c$  instead. Up to rotation of the axes this is exactly what is observed during the change in topology of the two TW in, for example, Figs. 5(e) and 5(f). A particularly nice example of this type of transition

occurs in the transition between Figs. 7(d) and 7(e), as discussed in Sec. 3.3 (see Fig. 8).

#### 4.5. The tangent bifurcation

Another type of bifurcation observed in Sec. 3 may be termed the tangent bifurcation. This bifurcation arises when the  $n = 1$  branch becomes tangent to the  $n = 2$  branch, as in Figs. 14(f) and 14(g), thereby introducing a pair of new steady state bifurcations on the latter and breaking the  $n = 1$  branch into two parts. This type of bifurcation can only occur when  $\beta > 0$  since it requires that the  $n = 1$  branch be a mixed mode branch in order that it can connect with the  $n = 2$  branch. The bifurcation is described by the normal form

$$\dot{z} = z(-\lambda^2 + \beta - \beta_c + z^2), \quad (13)$$

where  $\beta = \beta_c$  denotes the location of the tangency and  $z$  is a suitable measure of the amplitude of the  $n = 1$  component; this amplitude can be either positive or negative although both cases are identified in the figure. This normal form is nothing but the normal form in Sec. 4.2 but with the sign of the  $z^3$  term positive. As a result if  $\beta < \beta_c$  the solution  $z = 0$  is stable, but once  $\beta > \beta_c$  an unstable interval opens up between two steady state bifurcations. These bifurcations produce branches of solutions with

$|z| > 0$  and hence correspond to the  $n = 1$  solutions. In the present example [Figs. 14(f) and 14(g)] they are nothing but the  $R_1$  and  $R_2$  branches already encountered, and here they extend in opposite directions away from the origin  $(z, \lambda) = (0, 0)$  instead of forming a bubble. Once again, up to rotation of the axes, this is exactly what is observed during the tangent bifurcation that occurs between  $\beta = 0.148$  and  $\beta = 0.15$  in Figs. 14(f) and 14(g).

The same type of bifurcation also occurs in Figs. 10(a) and 10(b) between  $\beta = 0.8$  and  $\beta = 0.84$ . This time it is the branch of TW2 that becomes tangent to the  $n = 2$  branch, producing a doubly unstable segment on the latter. The corresponding normal form is identical to that in Eq. (13) with the replacement of  $z$  by the phase speed  $c$ . An identical bifurcation occurs in Figs. 7(e) and 7(f) when the disconnected large amplitude TW branch collides with the  $R_2$  branch, creating the bifurcation diagram in Fig. 7(f).

#### 4.6. The exchange bifurcation

As discussed in more detail in Sec. 3, when  $\sigma = 0.1$ ,  $\alpha = 2.18$  and  $\beta \approx 0.024$  the system undergoes a complex sequence of transformations, whose net effect is to interchange the bifurcation points  $M_0$  and  $M_\pi$  on  $n = 2$  [Figs. 7(d) and 7(e)], while the TW branch remains on the lower branch. A transition of this type is described by the normal form (7) but with  $A < 0$ ,  $B > 0$ ,  $A + 2B > 0$ . Moreover,  $\varepsilon > 0$  when  $\beta < \beta_c$  and vice versa. Once again increasing  $\lambda$  corresponds to decreasing  $Ra$ . At  $\varepsilon = 0$  the  $R$ -symmetric branch  $(a_1, 0)$  and the  $\rho^2 R$ -symmetric branch  $(0, a_2)$  coincide (i.e.  $a_1 = a_2 = a$ ) and these bifurcate from the  $n = 2$  branch together with the branch  $(a, a)$ . Both branches are subcritical, with the latter doubly unstable. When  $\varepsilon > 0$  ( $\beta < \beta_c$ ) the  $(a_1, 0)$  branch is encountered first as  $\lambda$  increases, followed by the  $(0, a_2)$  branch from which the TW branch  $(a_1, a_2)$  bifurcates. As  $\varepsilon$  decreases through zero the branches  $(a_1, 0)$  and  $(0, a_2)$  pass through one another with the bifurcation to the TW transferred to  $(a_1, 0)$ . Although the results of this analysis, including the stability assignments, are in complete agreement with the observed transition from Fig. 7(d) to Fig. 7(e), the detailed results reported in Sec. 3 reveal that the details of the transition are in fact more involved. Specifically as  $\beta$  increases we observe the formation of a TW bubble on the branch  $R_2$ , followed by necking (see Fig. 8), and then the motion of the bifurcation to TW on the

$R_2$  branch towards the  $n = 2$  branch, followed by the reemergence of this point on the new  $R_2$  once  $\beta$  exceeds  $\beta_c$ . In other words, the observed transition, for  $\beta$  sufficiently close to  $\beta_c$  is of the opposite type, with the TW bifurcating from  $(a_1, 0)$  instead of  $(0, a_2)$  as in the scenario just described. Clearly, close enough to  $\beta = \beta_c$  the coefficient  $A > 0$ , but it is small enough that further away from the bifurcation where higher order terms become important the system behaves *as if*  $A$  were in fact negative. It follows, therefore, that an explanation of the observed detailed transition must be sought in the unfolding of the degeneracy  $A = 0$ . The effect of forced symmetry-breaking from  $D_4$  to  $D_2$  on this degeneracy was analyzed in detail by Crawford and Knobloch [1988], and this theory is directly relevant to our pdes when  $\beta \approx \beta_c$ . Indeed, Sec. 2.3 of this paper identifies a number of possible transitions (depending on fifth- and seventh-order terms, cf. [Knobloch, 1986]), of which one is precisely of the type we have found in the pdes (under time reversal). We conclude therefore that the observed transition from Fig. 7(d) to Fig. 7(e) is the consequence of an accidental degeneracy (here  $A \approx 0$ ), in addition to the requirement that  $\beta \approx \beta_c$  in order to bring the two branches  $R_1$  and  $R_2$  together. Thus strictly speaking the observed exchange bifurcation is of codimension *three*, in contrast to the situation in Sec. 4.1 which represents the unfolding of a codimension-one degeneracy.

#### 4.7. The hysteresis bifurcation

When  $\sigma = 0.1$ ,  $\alpha < \alpha_c$ , a hysteresis (or cusp) bifurcation takes place on the  $n = 1$  branch between  $\beta = 10^{-4}$  and  $\beta = 0.14$ , creating a pair of saddle-node bifurcations on the  $n = 1$  branch [Fig. 14(b)]. This bifurcation is described by the normal form

$$\dot{z} = \lambda + \varepsilon z - z^3,$$

so that when  $\varepsilon < 0$  ( $\beta < \beta_c$ ) there is no hysteresis as  $\lambda$  increases, but a hysteresis loop is created as soon as  $\varepsilon > 0$  ( $\beta > \beta_c$ ).

#### 4.8. The saddle-node pitchfork

In Sec. 3 we located several instances where different codimension-two bifurcations take place. For example, in Figs. 7(f) and 7(g), the pitchfork to TW on the  $n = 1$  branch slides past the saddle-node bifurcation, creating a tertiary Hopf on the

TW branch. This bifurcation is described by the normal form

$$\dot{z} = -\lambda - z^2 + bc^2 + \mathcal{O}(3), \quad \dot{c} = -\mu c + azc + \mathcal{O}(3),$$

with  $a < 0$ ,  $b > 0$ . Here the symbol  $\mathcal{O}(3)$  indicates terms of cubic order required to resolve certain degeneracies involving the periodic oscillations present in these equations [Guckenheimer & Holmes, 1990]. Thus the states  $(z, 0)$  representing the amplitude of the  $n = 1$  branch near the saddle-node bifurcation are present for  $\lambda < 0$ , while the pitchfork to TW ( $c \neq 0$ ) occurs on the  $z < 0$  branch when  $\mu > 0$ , but as  $\mu$  passes through zero the TW pitchfork moves onto the  $z > 0$  branch; a (tertiary) Hopf bifurcation on the TW branch appears at the same time, as in Fig. 7(g). Note that the fate of the limit cycle created at the (tertiary) Hopf bifurcation falls outside the range of validity of the normal form, and may therefore involve global bifurcations with other states not described by the normal form. Recent work by Porter and Knobloch [2001] indicates some of the possibilities, and describes the complex dynamics that may result.

A different example can be seen in Figs. 14(b) and 14(d), where the bifurcation to the TW branch moves down past the larger amplitude saddle-node bifurcation as  $\beta$  increases, and coincides with it at  $\beta_c$ ,  $0.140 < \beta_c < 0.142$  ( $\alpha = 1.99$ ). Here the  $n = 1$  states are present for  $\lambda > 0$ , i.e. towards larger  $Ra$ , while the states above (below) the pitchfork are stable (unstable) to TW perturbations. The resulting bifurcation is described by the normal form,

$$\dot{z} = \lambda - z^2 + bc^2 + \mathcal{O}(3), \quad \dot{c} = \mu c + azc + \mathcal{O}(3),$$

with  $a < 0$ ,  $b < 0$ . In contrast to the case just described in this case no (tertiary) Hopf bifurcation appears as a result of this interaction. The origin of the standing waves indicated in Figs. 14(b) and 14(c) is quite different, and is discussed in Sec. 4.11 below.

#### 4.9. *The subharmonic bifurcation for traveling waves*

For  $\sigma = 0.1$  [Figs. 10(a)–10(d)] we encountered several instances of a subharmonic bifurcation of traveling waves. This bifurcation can be understood in terms of an interaction between two traveling waves with wavenumbers  $n = 2$  and  $n = 1$ . Recall that the former is invariant under the translation  $T_{L/4}$  followed by evolution through a time  $P/4$ , where  $P$  is

the time taken to travel the length  $L$ . Immediately after the bifurcation the symmetry of the TW will be  $T_{L/2}$  followed by evolution through a time  $P/2$ , i.e. the bifurcation is a subharmonic bifurcation in time as well and so is a standard period-doubling bifurcation. In the rest frame of the  $n = 2$  wave this bifurcation is a steady state bifurcation, and is indicated as such in the bifurcation diagrams. A relevant model problem of this type is provided by the equations describing the double Hopf bifurcation with 1:2 resonance (cf. [Knobloch & Proctor, 1988]),

$$\begin{aligned} \dot{a}_1 &= \lambda_1 a_1 + p_1 |a_1|^2 a_1 + q_1 |a_2|^2 a_1 + r_1 a_2 \bar{a}_1, \\ \dot{a}_2 &= \lambda_2 a_2 + p_2 |a_2|^2 a_2 + q_2 |a_1|^2 a_2 + r_2 a_1^2, \end{aligned}$$

where  $\lambda_j$ ,  $p_j$ ,  $q_j$ ,  $r_j$  ( $j = 1, 2$ ) are complex coefficients, and indicates that under appropriate conditions on the coefficients the pure  $n = 2$  branch (i.e. the branch consisting of solutions of the form  $(a_1, a_2) = (0, a_2)$ ) undergoes a secondary bifurcation to a mixed state of the form  $(a_1, a_2)$ ,  $a_1 a_2 \neq 0$ , and that this bifurcation is indeed subharmonic in time [Knobloch & Proctor, 1988].

#### 4.10. *The double pitchfork bifurcation*

The diagrams for  $\sigma = 0.1$  indicate that as  $\beta$  increases the  $n = 2$  branch is destabilized at large amplitude by the appearance of a bifurcation to TW2, i.e. with respect to traveling waves with only the wavenumber  $n = 2$  (Fig. 10). This TW2 branch undergoes a subharmonic instability of the type just described, with the resulting TW connecting to the  $R_2$  branch. The TW2 branch then undergoes a tangent bifurcation with the  $n = 2$  branch, as described in Sec. 4.5 above, that introduces two new bifurcations on the  $n = 2$  branch, both below the pitchfork to  $R_2$ . The upper of these then moves up along the  $n = 2$  branch [Figs. 10(a) and 10(b)] producing a double pitchfork on the  $n = 2$  branch when it collides with the pitchfork to  $R_2$ ; the subharmonic TW branch is eliminated in this process, i.e. as the two pitchforks on the  $n = 2$  branch approach one another both (tertiary) bifurcations generating TW move towards the  $n = 2$  branch. This behavior is seen quite clearly in Figs. 11(b) and 11(c) which show that the branch labeled TW( $R_2$ ) is eliminated when the solid circle that indicates its appearance collides with the axis  $c = 0$  (i.e. the steady  $n = 2$  branch). This behavior is readily understood by

examining the unfolding of the double pitchfork bifurcation,

$$\begin{aligned}\dot{z} &= \lambda z + Az^3 + Bc^2z, \\ \dot{c} &= (\lambda - \varepsilon)c + Cz^2c + Dc^3.\end{aligned}$$

Here  $z$  denotes the amplitude of the  $n = 1$  contribution, and  $c \neq 0$  indicates a traveling wave. Comparison with Figs. 10(b) and 10(c) indicates that we must take  $A > 0$ ,  $D > 0$ ,  $C > A$ ,  $B < D$  and  $AD - BC < 0$ . This is case Ib in the classification of Guckenheimer and Holmes [1990]. Starting from negative values of  $\lambda$ , i.e. from the stable part of the  $n = 2$  branch, and increasing  $\lambda$  (decreasing  $Ra$ ) with  $\varepsilon < 0$  (i.e.  $\beta > \beta_c$ ), we first encounter a subcritical bifurcation to TW2, followed by a second subcritical bifurcation to  $R_2$ . If  $\varepsilon > 0$  ( $\beta < \beta_c$ ) we find instead that the first bifurcation is to a subcritical  $R_2$  state which undergoes a further bifurcation to a once unstable ‘‘mixed mode’’. This mode is the TW branch, i.e. the TW branch that contains contributions from wavenumber  $n = 1$ . This branch terminates on the TW2 branch that bifurcates from the  $n = 2$  state at  $\lambda = \varepsilon$ , also subcritically.

#### 4.11. *A Takens–Bogdanov–pitchfork interaction*

There remains one aspect of the bifurcation diagrams reported in Sec. 3 that requires a more complicated analysis. This concerns the appearance between the two saddle-node bifurcations on the  $n = 1$  branch in Fig. 14(d) of an unexpected Hopf bifurcation to a reflection-symmetric state we have labeled SW. This Hopf bifurcation is not required (see Sec. 4.8 above); however, the fact that it is present calls for an explanation. A careful numerical investigation of the case  $\alpha = 1.99$  indicates that at  $\beta = 0.14$  the TW bifurcates from the  $n = 1$  branch above the upper saddle-node bifurcation, while at  $\beta = 0.142$  the bifurcation is below it. Thus the saddle-node–pitchfork interaction, discussed in Sec. 4.8 takes place at  $\beta_c$ ,  $0.14 < \beta_c < 0.142$ . At  $\beta = 0.143$  the Hopf bifurcation is still absent but it appears once  $\beta$  is increased to  $\beta = 0.144$  and falls between the saddle-node and pitchfork bifurcations [Fig. 14(d)]. From the motion of the eigenvalues it is clear that there are three eigenvalues that are responsible for these bifurcations, suggesting that only a third-order system is capable of providing a consistent explanation. We focus here on the

Takens–Bogdanov bifurcation on the  $n = 1$  branch coupled with a pitchfork to TW. This bifurcation is described by the normal form

$$\begin{aligned}\ddot{x} &= -(\nu - kx)\dot{x} - (\lambda - x^2) \pm y^2, \\ \dot{y} &= -(\mu - \gamma x)y\end{aligned}\tag{14}$$

(cf. [Arnéodo *et al.*, 1985]). Here  $x$  represents the variable in the reflection-invariant subspace, while  $y$  represents the variable associated with the traveling wave instability. Setting  $y = 0$  we see immediately that there is a saddle-node bifurcation at  $\lambda = 0$ , with a pair of equilibria  $(x_0, 0)$ ,  $x_0 = \pm\sqrt{\lambda}$ , for  $\lambda > 0$ . Of these the upper (+) equilibrium is a saddle while the lower (–) is stable if  $\nu > 0$  (cf. Fig. 14). Moreover, the lower equilibrium undergoes a pitchfork to TW, i.e. to equilibria of the form  $(x_0, y_0)$ ,  $x_0y_0 \neq 0$ , provided  $\gamma < 0$ . This bifurcation is supercritical (subcritical) if the sign of the last term is + (–). Finally, a Hopf bifurcation within the invariant space  $y = 0$  (i.e. to standing waves) occurs on the lower equilibrium provided  $k < 0$ . This bifurcation lies between the saddle-node and the pitchfork to traveling waves provided  $\gamma\nu > \mu k$ . Under these conditions (and the choice of the lower sign in the last term of the first equation) the resulting bifurcation diagram is of the type shown in Figs. 14(d), 14(f) and 14(h). Although the case just described is by no means the most interesting regime described by Eq. (14) it does provide a complete explanation of the transitions reported in Fig. 14 near  $\beta = 0.145$ , and indicates that we must take the parameter  $\nu = k_0(\beta - \beta_c)$ ,  $k_0 > 0$ , in order to take the system from Fig. 14(b) to Fig. 14(d).

## 5. Discussion

In this paper we have described the results of numerical branch-following techniques applied to the partial differential equations describing two-dimensional Rayleigh–Bénard convection in the vicinity of a codimension-two point at which two modes, with wavenumbers  $\alpha$  and  $2\alpha$  are simultaneously unstable. This technique allows us to compute all the branches of time-independent states that emanate from this point, as well as those corresponding to traveling waves, that is, states that are time-independent in an appropriately moving reference frame. We have focused on two values of the Prandtl number,  $\sigma = 10$  and  $\sigma = 0.1$ , characteristic of large and small Prandtl number regimes, respectively, exploring in each case the effect of chang-

ing the velocity boundary condition at the top of the layer from no-slip to stress-free while the lower boundary remained no-slip. This change in the boundary condition was accomplished via the introduction of a homotopy parameter which we have called  $\beta$ . Such homotopic continuation has been used before and has shed much light on the relationship between the bifurcation diagrams for superficially quite different problems [Schaeffer, 1980]. In the present problem, we described in detail for both Prandtl numbers the sequence of transitions through which the system passes as  $\beta$  varies from  $\beta = 0$  (no-slip) to  $\beta = 1$  (free-slip), and showed that these depend on whether  $\alpha > \alpha_c$  or  $\alpha < \alpha_c$ , i.e. on whether the imposed spatial period is smaller or larger than that corresponding to the codimension-two point. Since we have fixed the temperatures at the top and bottom boundaries and ignored all non-Boussinesq effects the partial differential equations studied possess a reflection symmetry with respect to the layer midplane when  $\beta = 0$  but this symmetry is broken when  $\beta > 0$ . Thus the homotopic continuation performed can be viewed alternatively as a study of the effects of a progressive increase in asymmetry between the boundary conditions imposed at the top and bottom of the layer.

Our study builds on our earlier work [Mercader *et al.*, 2001a] on the effects of weak symmetry breaking on the 1:2 resonance and reveals a definite sequence of additional bifurcations that must take place before the  $\beta = 0$  bifurcation diagram is transformed into the corresponding  $\beta = 1$  diagram. We have discussed each of these bifurcations in turn, using appropriate normal forms. Some of the bifurcations we identified were unexpected, such as the “necking” bifurcation (Sec. 4.4) or the Takens–Bogdanov–pitchfork interaction (Sec. 4.11). However, in all cases the study enabled us to understand the transition from the diagram of Fig. 2(a) to that in Fig. 2(d) ( $\alpha > \alpha_c$ ) and from Fig. 4(a) to that in Fig. 4(h) ( $\alpha < \alpha_c$ ) when  $\sigma = 10$ , and from Fig. 7(a) to that in Figs. 12(a) and 12(b) ( $\alpha > \alpha_c$ ) and from Fig. 13(a) to that in Figs. 15(a) and 15(b) ( $\alpha < \alpha_c$ ) when  $\sigma = 0.1$ . Of particular interest is the discovery of certain ranges of  $\beta$  within which there are intervals of Rayleigh numbers for which none of the simple states we compute are stable. In these intervals the partial differential equations must admit solutions with a more complex time-dependence, perhaps quasiperiodic or chaotic. In other cases we were able to identify the presence of a Hopf bifurcation to standing waves but have not followed the

resulting solution branch at finite amplitude. In a related paper [Mercader *et al.*, 2001b] we study the possibility of complex behavior identified here via direct numerical simulation of the governing partial differential equations, and explore other mechanisms for breaking the up-down symmetry, such as introducing a Biot number into the thermal boundary condition at the top to describe heat loss from the surface. Similar stability “gaps” are present in this case, allowing us to vary the Biot number to locate regimes with complex time-dependence in a system which exhibits none when the top surface is either perfectly conducting or perfectly insulating.

## Acknowledgments

This work was supported in part by DGESIC under grant PB97-0683 (I. Mercader and J. Prat) and by the National Science Foundation under grant DMS-9703684 (E. Knobloch). We thank the Fulbright Foundation for additional support. Some of the numerical results were obtained using CESCA and CEPBA infrastructure support coordinated by C<sup>4</sup>.

## References

- Armbruster, D. [1987] “O(2)-symmetric bifurcation theory for convection rolls,” *Physica* **D27**, 433–439.
- Armbruster, D., Guckenheimer, J. & Holmes, P. [1988] “Heteroclinic cycles and modulated traveling waves in systems with O(2) symmetry,” *Physica* **D29**, 257–282.
- Arnéodo, A., Coulet, P. H., Spiegel, E. A. & Tresser, C. [1985] “Asymptotic chaos,” *Physica* **D14**, 327–347.
- Bergeon, A., Henry, D. & Knobloch, E. [2001] “Three-dimensional Marangoni–Bénard flows in square and nearly square containers,” *Phys. Fluids* **13**, 92–98.
- Busse, F. H. [1967] “The stability of finite amplitude cellular convection and its relation to an extremum principle,” *J. Fluid Mech.* **30**, 625–649.
- Busse, F. H. & Or, A. C. [1986] “Subharmonic and asymmetric convection rolls,” *Z. Angew. Math. Phys.* **37**, 608–623.
- Clever, R. M. & Busse, F. H. [1996] “Hexagonal convection cells under conditions of vertical symmetry,” *Phys. Rev.* **E53**, R2037–R2040.
- Cox, S. M. [1996] “Mode interactions in Rayleigh–Bénard convection,” *Physica* **D95**, 50–61.
- Crawford, J. D. & Knobloch, E. [1988] “On degenerate Hopf bifurcation with broken O(2) symmetry,” *Nonlinearity* **1**, 617–652.
- Crawford, J. D. & Knobloch, E. [1991] “Symmetry and symmetry-breaking bifurcations in fluid mechanics,” *Ann. Rev. Fluid Mech.* **23**, 341–387.

- Golubitsky, M. & Schaeffer, D. G. [1988] *Singularities and Groups in Bifurcation Theory*, Vol. 1 (Springer-Verlag, NY).
- Golubitsky, M., Swift, J. W. & Knobloch, E. [1984] “Symmetries and pattern selection in Rayleigh–Bénard convection,” *Physica* **D10**, 249–276.
- Guckenheimer, J. & Holmes, P. [1990] *Nonlinear Oscillations, Dynamical Systems and Bifurcations of Vector Fields* (Springer-Verlag, NY).
- Jones, C. A. & Proctor, M. R. E. [1987] “Strong spatial resonance and travelling waves in Bénard convection,” *Phys. Lett.* **A121**, 224–228.
- Knobloch, E. [1986] “On the degenerate Hopf bifurcation with  $O(2)$  symmetry,” in *Multiparameter Bifurcation Theory*, eds. Golubitsky, M. & Guckenheimer, J., Contemporary Mathematics, Vol. 56 (American Mathematical Society, Providence, RI), pp. 193–201.
- Knobloch, E. & Proctor, M. R. E. [1988] “The double Hopf bifurcation with 2:1 resonance,” *Proc. R. Soc. London* **A415**, 61–90.
- Knobloch, E. & Moore, D. R. [1990] “A minimal model of binary fluid convection,” *Phys. Rev.* **A42**, 4693–4709.
- Knobloch, E. [1996] “Symmetry and instability in rotating hydrodynamic and magnetohydrodynamic flows,” *Phys. Fluids* **8**, 1446–1454.
- Manogg, G. & Metzener, P. [1994] “Strong resonance in two-dimensional non-Boussinesq convection,” *Phys. Fluids* **6**, 2944–2955.
- Matthews, P. C., Hurlburt, N. E., Proctor, M. R. E. & Brownjohn, D. P. [1992] “Compressible magnetoconvection in oblique fields: Linearized theory and simple nonlinear models,” *J. Fluid Mech.* **240**, 559–569.
- Mercader, I., Prat, J. & Knobloch, E. [2001a] “The 1:2 mode interaction in Rayleigh–Bénard convection with weakly broken midplane symmetry,” *Int. J. Bifurcation and Chaos* **11**(1), 27–41.
- Mercader, I., Prat, J. & Knobloch, E. [2001b] “Robust heteroclinic cycles in two-dimensional Rayleigh–Bénard convection without Boussinesq symmetry,” preprint.
- Moore, D. R., Weiss, N. O. & Wilkins, J. M. [1991] “Asymmetric oscillations in thermosolutal convection,” *J. Fluid Mech.* **233**, 561–585.
- Porter, J. & Knobloch, E. [2001] “New type of complex dynamics in the 1:2 spatial resonance,” *Physica* **D159**, 125–154.
- Prat, J., Massaguer, J. M. & Mercader, I. [1995] “Large-scale flows and resonances in 2-D thermal convection,” *Phys. Fluids* **7**, 121–134.
- Prat, J., Mercader, I. & Knobloch, E. [1998] “Resonant mode interactions in Rayleigh–Bénard convection,” *Phys. Rev.* **E58**, 3145–3156.
- Proctor, M. R. E. & Jones, C. A. [1988] “The interaction of two spatially resonant patterns in thermal convection. Part 1. Exact 2:1 resonance,” *J. Fluid Mech.* **188**, 301–335.
- Schaeffer, D. G. [1980] “Qualitative analysis of a model for boundary effects in the Taylor problem,” *Math. Proc. Camb. Phil. Soc.* **87**, 307–337.
- van Gils, S. & Mallet-Paret, J. [1986] “Hopf bifurcation and symmetry: Travelling and standing waves on the circle,” *Proc. R. Soc. Edinburgh* **A104**, 279–307.
- Weiss, N. O. [1990] “Symmetry breaking in nonlinear convection,” in *Nonlinear Evolution of Spatio-Temporal Structures in Dissipative Continuous Systems*, eds. Busse, F. H. & Kramer, L. (Plenum Press, NY), pp. 359–374.